THE JOURNAL
OF
CHEMICAL PHYSICS

VOLUME 10 MARCH, 1942 NUMBER 3

X-Ray Interference in Partially Ordered Layer Lattices‡

STERLING HENDRICKS, *United States Bureau of Plant Industry, Washington, D. C.*,
AND
EDWARD TELLER,* *The George Washington University, Washington, D. C.*
(Received October 30, 1941)

The x-ray interference is calculated for layer lattices in which the phase shifts between consecutive layers and the scattering powers of individual layers do not follow a strictly periodic arrangement. In the second section the scattering power of all layers is assumed to be the same but the phase shifts can take on different values. In the third section neither the scattering powers nor the phase shifts have fixed values but a simplifying assumption is made about the phase shifts according to which distances between neighboring layers can be represented as sums of two distances characteristic of the individual layers. In both these sections a random sequence of the layers is assumed. In the fourth section the problem of arbitrary scattering powers and phase shifts is treated, and furthermore a statistical correlation between neighboring layers is introduced. In the following section the general theory is applied to a specific partially ordered stacking of layers encountered in micas and other similar minerals. The last section treats irregularities in close packed structures of spheres and irregular sequences of layers in graphite.

SECTION 1

MANY crystals can be considered as being built up of a set of parallel layers. This picture is particularly useful if the forces acting within layers are greater than those acting between layers. The layers may be monatomic as in graphite or they may be several atoms deep as in micas and clay minerals. Even when the forces between layers are great the picture is still fruitful as shown by the usual comparison of hexagonal and cubic close packing.

X-ray investigations of some layer crystals have led to the conclusion that they are not completely ordered. The lack of order may be due to translations of the layers parallel to their own planes or to irregular sequence of layers of different kinds. These lattice irregularities may be manifested by changes in intensities of interferences in the x-ray diffraction pattern by diffuse scattering, or by broadening of the interference spots. The purpose of this paper is to calculate some of these effects for various kinds of irregularities.

For the purpose of calculations layers will be treated as having form factors. These factors vary with wave-length and with the orientation and direction of polarization of the incident and outgoing radiation relative to the plane of the layer. The layer form factor is analogous to the atom form factor but while the latter varies

‡ After completion of the manuscript it has come to the attention of the authors that questions similar to those discussed below have been treated by Landau and by Lifschitz. Their work will be described at the end of Section I.

* At present at Columbia University, New York, New York.

smoothly and monotonously with angle the former shows sharp discrete maxima due to the infinite extension of the layers in two directions. Layer form factors have been calculated by adding the scattering from the atoms within the layers.[1]

The amplitude of the radiation scattered by the crystal may be obtained by adding the amplitudes scattered by the individual layers. This reduces the calculation to a single summation over layer form factors and thus leads to a one-dimensional problem. The mathematical methods used can equally well be applied to the calculation of reflections from a single layer consisting of parallel but otherwise not strictly regular sequence of atomic chains. Again the scattering from a chain with irregular sequence of atoms could be calculated in the same manner. Practical applications, however, are limited to layer lattices.

Only problems will be treated in which there is some phase relation between scattering from different layers. If no such phase relation exists the total intensity is obtained by adding the intensities from the individual layers.[1,2]

In the second section it is assumed that all the layers have the same form factor. The phase shifts of radiation scattered by neighboring layers are supposed to have a limited number of values. Each phase shift occurs with a certain probability but there is no correlation between consecutive phase shifts. A practical example for which the above assumptions are approximately valid is the x-ray scattering from the hydrated clay mineral montmorillonite.[3] In this mineral identical layers containing heavy atoms are separated by varying numbers of water layers of considerably smaller scattering power. If we assume that the number of adjacent water layers is limited and if we neglect the scattering by water layers the influence of the water will be to produce a limited number of phase shifts between the scattering waves of neighboring heavy layers. The calculation yields intensity fluctuations rather than sharp interference maxima corresponding to orders of reflection.

In the third section crystals are considered which consist of layers with different form factors. It is assumed that each type of layer has a definite probability of occurrence, but the sequence of layers is random. Distances between neighboring layers and correspondingly their phase shifts depend upon the kind of layer. In order to obtain an explicit expression for the x-ray interference it is further assumed that the distance between two neighboring layers is a sum of two lengths characteristic of the layers. This assumption is satisfied if crystal distances can be obtained from ionic radii. A practical example is the precipitation of copper in a duralumin alloy in which the copper segregates on (100) planes of the crystal. Another example is afforded by the basic salts of the divalent metals, for instance $n\ CdCl_2 \cdot m\ Cd(OH)_2$. Here $CdCl_2$ and $Cd(OH)_2$ layers may follow each other in a random sequence.

In the fourth section a more general problem is treated than in the third. It is no longer assumed that distances between neighboring layers are sums of two characteristic lengths. Furthermore, a correlation between occurrence of layers is introduced such that the probability of a layer to be present in a certain position depends upon the neighboring layers as well as on the abundance of the layer in question. This correlation affords a transition between the case of a random sequence and a completely ordered crystal. This problem is not solved explicitly but is only given in terms of the solution of a secular equation of the nth order where n is the number of different kinds of layers. The practical examples are the same as given in the preceding sections only that a more exact and more laborious solution is offered.

In the final two sections the secular determinants are solved and intensities of interference explicitly given for two cases to which the treatment of Section 4 applies. The first of these is the stacking of layers in micas, kaolinite, etc. All layers have the same form factor but they may occupy any of three positions differing by shifts parallel to the plane of the layer. This is possible since relative positions of neighboring atoms in the top of one layer and the bottom of another are not affected by such shifts. Probabilities are assumed for each possible relative shift of neighboring layers. The second example treats irregularities in close packed structures of spheres and

[1] M. von Laue, Zeits. f. Krist. **82**, 127 (1932).
[2] B. E. Warren, Phys. Rev. **59**, 693 (1941).
[3] S. B. Hendricks, R. A. Nelson, and L. T. Alexander, J. Am. Chem. Soc. **2**, 1457 (1940).

irregular sequences of layers in graphite. In both these cases regular packing obtains for neighboring layers and irregularities enter only in relationships of second neighbors. Nevertheless the problem can be reduced to the one treated in Section 4. Neither of these cases has yet been observed[7] but the occurrence of the graphite case is to be expected since there is evidence for perfectly random shifts parallel to the planes of the layers in some crystals.

Influences of finite size of crystallites, thermal motion, divergence of x-ray beams, and the dynamical interference theory are not considered in this paper.

Two publications by Landau and by Lifschitz[4] give explicit intensity formulae for several types of arrangements of layers assuming no correlation between the layers. The following Section 2 of the present paper gives a somewhat more general treatment of the same problem. The influence of the correlation between layers has been considered later by Lifschitz[5] for the special case that the crystal consists of two kinds of layers. The calculations given in the first part of Section 4 of the present paper deal with the same problem. These calculations have been included merely as an introduction to the treatment of crystals containing several kinds of layers.

SECTION 2

It is assumed that all layers have the same form factor. For the sake of simplicity the case where only two phase shifts, φ_1, and φ_2, may occur between neighboring layers will be considered first. The frequency of occurrence of the two phase shifts is assumed to be equal and the sequence of the phase shifts is random. The alternation of phase shifts between two values may be due either to displacements of the layers parallel or perpendicular to their planes.

The amplitude and phase of the scattered radiation is represented by a vector in the complex plane

$$|\mathbf{V}| = |V| \exp i\varphi,$$

where V is the amplitude of the wave and φ stands for its phase. If $\mathbf{V}_k$ represents the scattering from the kth plane the scattering from a crystal consisting of n planes is

$$\sum_1^n k\, \mathbf{V}_k.$$

The absolute square of this sum gives the intensity. The intensity per layer is

$$I = \frac{1}{n} \sum_1^n k \sum_1^n l\, \mathbf{V}_k \cdot \mathbf{V}_l^*,$$

where $\mathbf{V}_l^*$ is the conjugate complex of $\mathbf{V}_l$. If n approaches infinity one may replace the double summation and subsequent division with n by a single summation in which the product of one vector with every other vector of the lattice appears. Thus

$$I = (\tfrac{1}{2}) \sum_{-\infty}^{+\infty} k(\mathbf{V}_k\mathbf{V}_0^* + \mathbf{V}_k^*\mathbf{V}_0) = \sum_{-\infty}^{+\infty} k\, |V_k|\, |V_0| \cos(\varphi_k - \varphi_0). \tag{1}$$

Here $(\varphi_k - \varphi_0)$ may be written as

$$(\varphi_k - \varphi_0) = (\varphi_k - \varphi_{k-1}) + (\varphi_{k-1} - \varphi_{k-2}) + \cdots (\varphi_1 - \varphi_0).$$

Each of these differences may have the values $\varphi^{(1)}$ or $\varphi^{(2)}$ with equal probability, where $\varphi^{(1)}$ and $\varphi^{(2)}$ are the two possible phase shifts between neighboring layers.

[4] L. Landau, Phys. Zeits. Soviet Union **12**, 579 (1937); I. M. Lifschitz *ibid.* **12**, 623 (1937).
[5] I. M. Lifschitz, J. Exper. Theor. Physics U. S. S. R., p. 500 (1939).

The average intensity per layer I_{Av} is obtained by averaging Eq. (3). Since the absolute values of the vectors are all equal the actual averaging need be carried out only over the cosines.

$$I_{Av}=\sum_{-\infty}^{+\infty}k[\,|V_k||V_0|\cos(\varphi_k-\varphi_0)]_{Av}=V^2\sum_{-\infty}^{+\infty}k[\cos(\varphi_k-\varphi_0)]_{Av}. \tag{2}$$

Here V^2 is the absolute square of the scattered vector for any layer, and the average over the sum has been replaced by the sum over the average values. Since

$$[\cos(\varphi_0-\varphi_0)]_{Av}=1,\quad [\cos(\varphi_k-\varphi_0)]_{Av}=[\cos(\varphi_{-k}-\varphi_0)]_{Av}, \tag{3}$$

the calculation need be carried out only for positive k values. Without loss of generality the phase of the scattered wave can be normalized in such a way that $\varphi_0=0$. If $\frac{1}{2}(\varphi^{(1)}+\varphi^{(2)})=\bar{\varphi}$ it follows that

$$[\cos\varphi_k]_{Av}=[\cos k\bar{\varphi}\cos(\varphi_k-k\bar{\varphi})-\sin k\bar{\varphi}\sin(\varphi_k-k\bar{\varphi})]_{Av}$$

$$=\cos k\bar{\varphi}[\cos(\varphi_k-k\bar{\varphi})]_{Av}-\sin k\bar{\varphi}[\sin(\varphi_k-k\bar{\varphi})]_{Av}.$$

The arguments $(\varphi_k-k\bar{\varphi})$ may assume values differing in sign only and such a pair occur with equal probabilities so that $[\sin(\varphi_k-k\bar{\varphi})]_{Av}=0$. Thus

$$[\cos\varphi_k]_{Av}=\cos k\bar{\varphi}[\cos(\varphi_k-k\bar{\varphi})]_{Av}. \tag{4}$$

The average values of the cosines can now be found by complete induction.

$$[\cos(\varphi_{k+1}-(k+1)\bar{\varphi})]_{Av}=[\cos(\varphi_k-k\bar{\varphi})\cos[(\varphi_{k+1}-\varphi_k)-\bar{\varphi}]]_{Av}$$

$$-[\sin(\varphi_k-k\bar{\varphi})\sin[(\varphi_{k+1}-\varphi_k)-\bar{\varphi}]]_{Av}. \tag{5}$$

Since there is no correlation between subsequent phase shifts the average over the factors of the right side may be carried out independently. The average over the sin terms vanish. According to the definition of $\bar{\varphi}$

$$(\varphi_{k+1}-\varphi_k)-\bar{\varphi}=\pm\tfrac{1}{2}(\varphi^{(1)}-\varphi^{(2)})$$

and by complete induction

$$[\cos(\varphi_k-k\bar{\varphi})]_{Av}=(\cos\tfrac{1}{2}(\varphi^{(1)}-\varphi^{(2)}))^k.$$

From (2), (3) and (4) it follows that

$$I_{Av}=V^2[1+2\sum_1^\infty k\cos k\bar{\varphi}(\cos\tfrac{1}{2}(\varphi^{(1)}-\varphi^{(2)}))^k]$$

$$=V^2[1+\sum_1^\infty k(\cos\tfrac{1}{2}(\varphi^{(1)}-\varphi^{(2)}))^k\exp ik\bar{\varphi}+\sum_1^\infty k(\cos\tfrac{1}{2}(\varphi^{(1)}-\varphi^{(2)}))^k\exp -ik\bar{\varphi}].$$

Evaluating the geometrical sums and writing the results with a common denominator I_{Av} is obtained as

$$I_{Av}=V^2\left[\frac{1-[\cos\frac{1}{2}(\varphi^{(1)}-\varphi^{(2)})]^2}{1-2\cos\bar{\varphi}\cos\frac{1}{2}(\varphi^{(1)}-\varphi^{(2)})+[\cos\frac{1}{2}(\varphi^{(1)}-\varphi^{(2)})]^2}\right]. \tag{6}$$

This formula gives in general a scattered intensity in every direction for which V is different from zero. The influence of the layer form factor, of course, is contained in V. If both $\varphi^{(1)}$ and $\varphi^{(2)}$ approach multiples of 2π at the same rate as their difference approaches 2π then Eq. (6) becomes infinite. In fact while the numerator approaches zero linearly the denominator approaches zero quadratically. This corresponds to a sharp interference maximum.

In order to illustrate intensity fluctuations given by Eq. (6) scattering of a layer lattice in which the distances of neighboring layers have the values 10A and 13A with equal probabilities will be

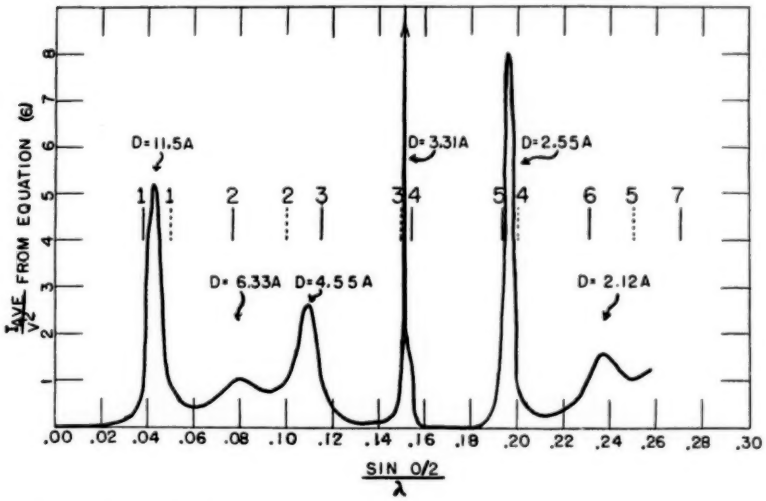

FIG. 1. Scattering from a random mixture of two layers having equal scattering power but different phase shifts corresponding to interlayer spacings of 10A and 13A. Angle of incidence equals one-half of scattering angle, θ. Results according to Eq. (6).

considered. This lattice corresponds to the partially hydrated montmorillonite where 10A obtains for the anhydrous material and 13A obtains if there is one water layer between two silicate layers. Figure 1 gives the intensity of reflections from the parallel set of planes as a function of $(\sin/\lambda)\theta/2$ where $\theta/2$ is the angle of incidence. The full perpendicular lines correspond to consecutive orders of reflections for a lattice with layers having 13A as their separation, while the dotted perpendicular lines refer to a lattice with a 10A constant. It is interesting to observe that the curve representing Eq. (6) shows marked maxima where sharp interference of these two crystals occurs near the same angle while lower and broader maxima are found for isolated interference maxima of the regular lattices. Of course no definite orders can be assigned to the intensity fluctuations in the curve. For $(\sin/\lambda)\theta/2=0.5A^{-1}$ the 13th order for the lattice with 13A separation and the 10th order for the 10A lattice coincide and at this point Eq. (6) becomes infinite corresponding to a sharp interference maximum. The actual substance seems to follow the behavior shown in Fig. 1.

In generalizing the above results it is assumed that r different phase shifts $\varphi^{(1)}, \varphi^{(2)}, \cdots, \varphi^{(r)}$ can occur between neighboring layers with frequencies $f^{(1)}, f^{(2)}, \cdots, f^{(r)}$. Since one of these phase shifts must be present between any two neighboring layers the sum of frequencies is

$$\sum_1^r s\, f^{(s)} = 1.$$

It will again be necessary to calculate Eq. (2) which amounts to calculating $[\cos(\varphi_k-\varphi_0)]_{Av}$. Eq. (1) remains valid but each term on the right-hand side might have any of the values $\varphi^{(s)}$ $(s=1, 2, \cdots r)$. Essentially the same reasoning can be used as before. An average phase shift $\bar{\varphi}$ is defined by the implicit equation

$$\sum_1^r s\, f^{(s)} \sin(\varphi^{(s)}-\bar{\varphi}) = 0. \tag{7}$$

It is necessary to show that $[\sin(\varphi_k-k\bar{\varphi})]_{Av}=0$, a relation which in the previous case followed immediately from equal frequency of occurrence of positive and negative values of the argument for the sine. One finds

$$[\sin(\varphi_{k+1}-(k+1)\bar{\varphi})]_{Av}=[\sin[(\varphi_{k+1}-\varphi_k)-\bar{\varphi}]\cos(\varphi_k-k\bar{\varphi})+\cos[(\varphi_{k+1}-\varphi_k)-\bar{\varphi}]\sin(\varphi_k-k\bar{\varphi})]_{Av}.$$

The averaging can again be carried out independently over the factors. Since $(\varphi_{k+1}-\varphi_k)$ must have one of the values $\varphi^{(s)}$ with the frequency $f^{(s)}$ the average of the first factor in the first term on the right-hand side vanishes according to Eq. (7). Thus

$$[\sin(\varphi_{k+1}-(k+1)\bar{\varphi})]_{Av}=[\cos[(\varphi_{k+1}-\varphi_k)-\bar{\varphi}]\sin(\varphi_k-k\bar{\varphi}]]_{Av}$$

and it is apparent that $[\sin(\varphi_{k+1}-(k+1)\bar{\varphi}=0]_{Av}$ if $[\sin(\varphi_k-k\bar{\varphi})]_{Av}=0$. Since Eq. (7) means that $[\sin(\varphi_k-k\bar{\varphi})=0]_{Av}$ for $k=1$, one obtains by complete induction that $[\sin(\varphi_k-k\bar{\varphi})=0]_{Av}$ for any value of k.

Now Eq. (4) and a relation

$$[\cos(\varphi_{k+1}-(k+1)\bar{\varphi})]_{Av}=[\cos(\varphi_k-k\bar{\varphi})]_{Av}[\cos[(\varphi_{k+1}-\varphi_k)-\bar{\varphi}]]_{Av},$$

which is analogous to Eq. (5) follow in the same way as in the previous proof.

Introducing the abbreviation

$$[\cos((\varphi_{k+1}-\varphi_k)-\bar{\varphi})]_{Av}=\sum_1^r s\, f^{(s)}\cos(\varphi^{(s)}-\bar{\varphi})=C, \tag{8}$$

it can be shown by complete induction that

$$[\cos(\varphi_k-k\bar{\varphi})]_{Av}=C^k \quad \text{and} \quad [\cos\varphi_k]_{Av}=C^k\cos k\bar{\varphi}.$$

Equation (2) now assumes the form

$$I_{Av}=\frac{V^2[1-C^2]}{1-2C\cos\bar{\varphi}+C^2}.$$

This expression is the same as Eq. (6) only the quantity $\cos(\frac{1}{2})(\varphi^{(1)}-\varphi^{(2)})$ has been replaced by C and the quantity $\bar{\varphi}$ is defined by Eq. (7).

SECTION 3

A mixture of r kinds of layers differing in their form factors is now considered. The sequence of layers is random and, at first, it is assumed that the phase shift is the same between any two consecutive layers.

Considering a finite crystal of n layers the radiation scattered by the kth layer can be written as $\mathbf{V}^{(s)}\exp ik\varphi$; here $\mathbf{V}^{(s)}$ is the scattering vector descriptive for the rth kind of layer which is supposed to occupy the kth position. The quantity $\mathbf{V}^{(s)}$ depends of course on the directions and polarizations of the incident and scattered x-rays beams but it does not depend on the phase shift between layers. This latter dependence is contained in the factor $\exp ik\varphi$. It must be borne in mind that the $\mathbf{V}^{(s)}$ are in general complex, for instance translation within the plane of a layer multiplies the $\mathbf{V}^{(s)}$ by complex factors with the absolute value unity. The average intensity per layer can be written as

$$I_{Av}=\frac{1}{n}\sum_1^n k\sum_1^n l\,\mathbf{V}^{(s)}\mathbf{V}^{(t)*}\exp i(k-l)\varphi,$$

where $\mathbf{V}^{(t)*}$ is the scattering of the tth kind of layer which happens to occupy the lth position in the sequence. The averaging is to be performed over (s) and (t) each of which can independently take on values from 1 to r with frequencies $f^{(1)}, \cdots, f^{(r)}$ which again satisfy

$$\sum_1^r s\, f^{(s)}=1. \tag{9}$$

Thus the average intensity is

$$I_{Av}=\frac{1}{n}\sum_{1}^{n}{}'kl\sum_{1}^{r}st[\mathbf{V}^{(s)}\mathbf{V}^{(t)*}f^{(s)}f^{(t)}\exp i(k-l)\varphi+\frac{1}{n}\sum_{1}^{n}k\sum_{1}^{r}s\,f^{(s)}\,|\,V^{(s)}\,|^{2}], \tag{10}$$

where the prime on the first summation indicates that $k=l$ must be excluded. The occurrence of two sums is due to the fact that for $k\neq l$, $f^{(s)}$ and $f^{(t)}$ are independent probabilities while for $k=l$ both s and t describe the same layer. Since in the second sum on the right-hand side k does not occur under the summation sign, the summation over k giving simply a factor n which cancels the factor $1/n$.

The scattering vectors $\mathbf{V}^{(s)}$ can be considered as sums of two vectors

$$\mathbf{V}^{(s)}=\mathbf{U}+\mathbf{W}^{(s)}, \tag{11}$$

where $\mathbf{U}$ is an average scattering vector defined by

$$\mathbf{U}=\sum_{1}^{r}s\,f^{(s)}\mathbf{V}^{(s)}.$$

The $\mathbf{W}^{(s)}$ are then defined by Eq. (10). Multiplying both sides of Eq. (10) with $f^{(s)}$ and adding

$$\sum_{1}^{r}(s)\,f^{(s)}\mathbf{W}^{(s)}=0 \tag{12}$$

is obtained.

Substituting (10) into (9) shows that the average intensity can be written as a sum of three terms

$$I_{Av}=I_{uu}+I_{uw}+I_{ww},$$

where

$$I_{uu}=\frac{1}{n}\sum_{1}^{n}{}'kl\sum_{1}^{r}stf^{(s)}f^{(t)}\mathbf{U}\mathbf{U}^{*}\exp i(k-l)\varphi+\sum_{1}^{r}s\,f^{(s)}\,|\,U\,|^{2},$$

$$I_{uw}=\frac{1}{n}\sum_{1}^{n}{}'kl\sum_{1}^{r}stf^{(s)}f^{(t)}[\mathbf{U}\mathbf{W}^{(s)*}+\mathbf{W}^{(s)}\mathbf{U}^{*}]\exp i(k-l)\varphi+\sum_{1}^{r}s\,f^{(s)}(\mathbf{U}\mathbf{W}^{(s)*}+\mathbf{W}^{(s)}\mathbf{U}^{*}),$$

$$I_{ww}=\frac{1}{n}\sum_{1}^{n}{}'kl\sum_{1}^{r}stf^{(s)}f^{(t)}\mathbf{W}^{(s)}\mathbf{W}^{(t)*}\exp i(k-l)\varphi+\sum_{1}^{r}sf^{(s)}\,|\,W^{(s)}\,|^{2}.$$

In I_{uu} the summation over s and t gives according to Eq. (9)

$$I_{uu}=\frac{1}{n}\sum_{1}^{n}k\sum_{1}^{n}l\,|\,U\,|^{2}\exp i(k-l)\varphi \qquad (k=l \text{ not excluded}),$$

which is the same result as would be obtained for a completely regular layer lattice where all layers have the form factor U. The summation over s and t shows that the expression I_{uw} vanishes according to Eq. (12). The same holds for the first sum in I_{ww} while the term

$$\sum_{1}^{r}s\,f^{(s)}\,|\,W^{(s)}\,|^{2}$$

gives the average scattering of a single layer having scattering vectors $\mathbf{W}^{(s)}$ with probabilities $f^{(s)}$. Thus the two non-vanishing terms in I_{Av} correspond to the scattering from a completely regular lattice and to scattering uninfluenced by phase relations in which the angular dependence of the scattering is determined by the layer form factor alone. In other words the crystal behaves as though it were completely regular and had a form factor equal to the average of form factors and as though

there were present in addition layers scattering independently and having form factors equal to the deviation of each real form factor from the average. If only two kinds of layers are present it can easily be seen that in the latter kind of scattering the difference of form factors enters.

The results here obtained can readily be generalized to a random mixture of scattering centers in any kind of lattice. In fact phase relations do not enter explicitly in the argument and as long as phase relations are the same for all r kinds of scattering centers the above result remains valid. The results for the general case have actually been found by von Laue in 1918.[6] Thus the scattering from a completely random solid solution gives interference corresponding to the completely ordered crystal with an average form factor on which a continuum is superimposed with an intensity distribution that depends on the deviation of the individual atom form factors from the average. This continuum will have an appreciable value at zero angle.

An explicit formula for the scattering can be obtained even if it is assumed that the phase shift between two neighboring layers of the kinds s and t depends on the nature of these layers. But, a simple solution can be obtained only if this phase shift $\varphi^{(st)}$ is the sum of two phase shifts $\varphi^{(s)}$ and $\varphi^{(t)}$ characteristic of the separate layers; $\varphi^{(s)}$ and $\varphi^{(t)}$ will of course depend on angle of scattering as well as the wave-length of x-rays. The average intensity then becomes

$$I_{Av}=\left[\frac{1}{n}\sum_{1}^{n}k\sum_{1}^{n}l\,\mathbf{V}_k^{(s)}\mathbf{V}_l^{(t)*}\exp i\varphi_{(k-l)}\right]_{Av}, \tag{13}$$

where the subscripts k and l emphasize that the vector $\mathbf{V}_k^{(s)}$ is in the kth and the vector $\mathbf{V}_l^{(t)}$ in the lth position.

The angle $\varphi_{(k-l)}$ is the phase shift between the kth and lth layer. Since $\varphi_{(k-l)}$ depends not only on the nature of the kth and lth layer but also on the nature of the intervening layers the averaging cannot be replaced now by summations over the two layers involved but complete induction must be used as in the previous section.

Equation (13) can be transformed in the same way as the expression for the intensity was transformed in the beginning of Section 2. Writing $|\mathbf{V}^s|=|V^s|\exp i\alpha^{(s)}$ one obtains for

$$I_{Av}=\sum_{-\infty}^{+\infty}k\left[|V_k^{(s)}||V_0^{(t)}|\cos\left(\varphi_{(k-0)}+\alpha^{(s)}-\alpha^{(t)}\right)\right]_{Av}. \tag{14}$$

The summation now extends from $-\infty$ to $+\infty$ the crystal having been replaced as in the second section by an infinite sequence of layers. $\varphi_{(k-0)}$ is the phase shift between the kth and zeroth layers.

The average over the kth term in Eq. (14) will first be considered. Assume $k>0$ and start with the averaging over the $(k-1)$th layer by substituting all the possible kinds of layers into that position but leaving the other layers unchanged. Assuming that the $(k-1)$th layer is of the pth kind and the $(k-2)$nd layer is of the qth kind one may write

$$\varphi_{(k-0)}=\varphi_{((k-2)-0)}+\varphi^{(q)}+2\varphi^{(p)}+\varphi^{(s)}.$$

For the average value over the $(k-1)$th layer is obtained

$$\begin{aligned}\sum_{1}^{r}p\,f^{(p)}|V_k^{(s)}||V_0^{(t)}|\cos\left[\varphi_{((k-2)-0)}+\varphi^{(q)}+2\varphi^{(p)}+\varphi^{(s)}+\alpha^{(s)}-\alpha^{(t)}\right]\\ =\sum_{1}^{r}p\,f^{(p)}|V_k^{(s)}||V_0^{(t)}|\cos\left[\varphi_{((k-2)-0)}+\varphi^{(q)}+\varphi^{(s)}+\alpha^{(s)}-\alpha^{(t)}+\bar{\varphi}\right]\cos\left(2\varphi^{(p)}-\bar{\varphi}\right)\\ -\sum_{1}^{r}p\,f^{(p)}|V_k^{(s)}||V_0^{(t)}|\sin\left[\varphi_{((k-2)-0)}+\varphi^{(q)}+\varphi^{(s)}+\alpha^{(s)}-\alpha^{(t)}+\bar{\varphi}\right]\sin\left(2\varphi^{(p)}-\bar{\varphi}\right).\end{aligned} \tag{15}$$

[6] M. von Lane, Ann. d. Physik **56**, 497 (1918).

If in this expression $\bar{\varphi}$ is defined by the implicit relation

$$\sum_1^r p\, f^{(p)} \sin(2\varphi^{(p)} - \bar{\varphi}) = 0, \tag{16}$$

the second term on the right-hand side of Eq. (15) vanishes. Introducing the abbreviation

$$\sum_1^r p\, f^{(p)} \cos(2\varphi^{(p)} - \bar{\varphi}) = C \tag{17}$$

and performing the average over the remaining layers which have been kept fixed so far there results

$$[|V_k^{(s)}||V_0^{(t)}| \cos(\varphi_{(k-0)} + \alpha^{(s)} - \alpha^{(t)})]_{Av}$$
$$= [C|V_k^{(s)}||V_0^{(t)}| \cos(\varphi_{((k-2)-0)} + \varphi^{(q)} + \varphi^{(s)} + \alpha^{(s)} - \alpha^{(t)} + \bar{\varphi})]_{Av}. \tag{18}$$

Since $\varphi^{(q)} + \varphi^{(s)}$ would be the phase shift between a layer of the qth and sth kind if these layers were neighbors the factor by which C is multiplied in Eq. (18) differs from the average taken over a pair of layers in the positions 0 and $k-1$ only by the phase $\bar{\varphi}$ appearing in the cosine. One can, therefore, write

$$[|V_k^{(s)}||V_0^{(t)}| \cos(\varphi_{(k-0)} + \alpha^{(s)} - \alpha^{(t)})]_{Av} = [C|V^{(s)}{}_{(k-1)}||V_0^{(t)} \cos(\varphi_{((k-1)-0)} + \alpha^{(s)} - \alpha^{(t)} + \bar{\varphi})]_{Av}.$$

By complete induction it finally follows that

$$[|V_k^{(s)}||V_0^{(t)}| \cos(\varphi_{(k-0)} + \alpha^{(s)} - \alpha^{(t)})]_{Av} = [C^{(k-1)}|V_1^{(s)}||V_0^{(t)}| \cos\varphi_{(1-0)} + \alpha^{(s)} - \alpha^{(t)} + (k-1)\bar{\varphi})]_{Av}$$
$$= \sum_1^r s \sum_1^r t\, C^{(k-1)} f^{(s)} f^{(t)} |V_1^{(s)}||V_0^{(t)}| \cos(\varphi^{(s)} + \varphi^{(t)} + \alpha^{(s)} - \alpha^{(t)} + (k-1)\bar{\varphi}).$$

For negative k values the same expression is obtained except that $|k|$ rather than k appears in the formula. The contribution of the term with $k=0$ to Eq. (14) is

$$\sum_1^r s\, f^{(s)} |V^{(s)}|^2.$$

Thus is obtained

$$I_{Av} = \sum_1^r s\, f^{(s)} |V^{(s)}|^2 + 2 \sum_1^\infty k \sum_1^r st C^{(k-1)} f^{(s)} f^{(t)} |V^{(s)}||V^{(t)}| \cos(\varphi^{(s)} + \varphi^{(t)} + \alpha^{(s)} - \alpha^{(t)} + (k-1)\bar{\varphi}). \tag{19}$$

The cosine in the second term in Eq. (19) can be expressed in exponentials and the summation is then reduced to a geometrical series giving

$$I_{Av} = \sum_1^r s\, f^{(s)} |V^{(s)}|^2 + 2 \sum_1^r st\, f^{(s)} f^{(t)} |V^{(s)}||V^{(t)}|$$
$$\times \left\{ \frac{\cos(\varphi^{(s)} + \varphi^{(t)} + \alpha^{(s)} - \alpha^{(t)}) - C \cos(\varphi^{(s)} + \varphi^{(t)} - \bar{\varphi} + \alpha^{(s)} - \alpha^{(t)}}{1 - 2c \cos\bar{\varphi} + C^2} \right\}. \tag{20}$$

It is of interest to compare this formula with the one obtained in the first part of this section. In this case the $\varphi^{(s)}$ become equal to each other and to $\bar{\varphi}/2$. From Eq. (17) it follows that $C=1$. After breaking down $\mathbf{V}^{(s)}$ into $\mathbf{U}$ and $\mathbf{W}^{(s)}$ Eq. (20) can be transformed into two terms the one containing the $\mathbf{W}$'s and giving no interferences and the other containing $\mathbf{U}$ and giving sharp interference maxima.

SECTION 4

The case where the sequence of layers is no longer random, but where correlation between neighboring layers is introduced will now be considered. To illustrate the procedure to be followed in this case it will first be assumed that two kinds of layers occur with equal frequency and that the phase shift between neighboring layers is always the same. The layer form factors are real and have the values $V^{(1)}$ and $V^{(2)}$.

To introduce correlation between layers two neighboring layers are considered and it is assumed that the probabilities that a layer of the first kind is followed by a layer of the first kind is $A_1^{(11)}$, for a layer of the first kind by second kind $A_1^{(12)}$, for a layer of second by first kind $A_1^{(21)}$, and for second kind by second kind $A_1^{(22)}$. Since the first layer of the pair has a probability of $\frac{1}{2}$ to be of the first kind and $\frac{1}{2}$ to be of the second kind it follows that

$$A_1^{(11)}+A_1^{(12)}=\tfrac{1}{2}, \quad A_1^{(21)}+A_1^{(22)}=\tfrac{1}{2}.$$

Since the second layer of the pair has also the probability $\frac{1}{2}$ to be of the first or second kind one finds

$$A_1^{(11)}+A_1^{(21)}=\tfrac{1}{2} \quad \text{and} \quad A_1^{(12)}+A_1^{(22)}=\tfrac{1}{2}.$$

From these relations it follows that

$$A_1^{(12)}=A_1^{(21)} \quad \text{and} \quad A_1^{(11)}=A_1^{(22)}.$$

The following abbreviation is now introduced,

$$\begin{aligned} A_1^{(11)}&=A_1^{(22)}=\tfrac{1}{4}+A, \\ A_1^{(12)}&=A_1^{(21)}=\tfrac{1}{4}-A. \end{aligned} \tag{21}$$

The probability $P^{(11)}=2A^{(11)}$ that the second layer of a pair is of the kind one if the first is of the kind one is now introduced. Similarly

$$P^{(12)}=2A^{(12)}, \quad P^{(21)}=2A^{(21)}, \quad P^{(22)}=2A^{(22)}.$$

Then the correlations between second neighbors can be calculated by multiplying the P's. In fact, the probability for a third layer to be of the first kind if the first was of the first kind is

$$P_2^{(11)}=P_1^{(11)}\cdot P_1^{(11)}+P_1^{(12)}P_1^{(21)}$$

and the probability $A_2^{(11)}$ to find two layers of the first kind as second neighbors is given by

$$A_2^{(11)}=\tfrac{1}{2}P_2^{(11)}=2[A_1^{(11)}\cdot A_1^{(11)}+A_1^{(12)}\cdot A_1^{(21)}].$$

Similarly the probabilities of other combinations as second neighbors are

$$A_2^{(22)}=\tfrac{1}{2}P_2^{(22)}=2[A_1^{(22)}\cdot A_1^{(22)}+A_1^{(21)}\cdot A_1^{(12)}],$$

$$A_2^{(12)}=\tfrac{1}{2}P_2^{(12)}=2[A_1^{(11)}\cdot A_1^{(12)}+A_1^{(12)}\cdot A_1^{(22)}],$$

$$A_2^{(21)}=\tfrac{1}{2}P_2^{(21)}=2[A_1^{(22)}\cdot A_1^{(21)}+A_1^{(21)}\cdot A_1^{(11)}].$$

From Eq. (21) it follows that

$$A_2^{(11)}=A_2^{(22)}=\tfrac{1}{4}[1+(4A)^2],$$

$$A_2^{(21)}=A_2^{(12)}=\tfrac{1}{4}[1-(4A)^2].$$

In a similar manner the probabilities for any two kinds of layers occurring as kth neighbors, $A_k^{(11)}$, $A_k^{(22)}$, $A_k^{(12)}$, $A_k^{(21)}$ can be introduced. These probabilities can be reduced to the probabilities of finding 2 kinds of neighbors as $(k-1)$th layers by the relation

$$A_k^{(11)}=2(A^{(11)}{}_{(k-1)}\cdot A_1^{(11)}+A^{(12)}{}_{(k-1)}\cdot A_1^{(21)})$$

and three similar equations. One can easily verify that the equations for arbitrarily removed neighbors are satisfied by writing,

$$\begin{aligned} A_k^{(11)}&=A_k^{(22)}=\tfrac{1}{4}(1+(4A)^k, \\ A_k^{(21)}&=A_k^{(12)}=\tfrac{1}{4}(1-(4A)^k). \end{aligned} \tag{22}$$

For $k=0$ we have

$$A_0^{(11)}=A_0^{(22)}=\tfrac{1}{2}; \quad A_0^{(12)}=A_0^{(21)}=0$$

which may be interpreted as meaning that a layer cannot be of the kind 1 and 2 at the same time and has the probability $\frac{1}{2}$ of being either kind 1 or 2. Thus Eq. (22) holds even for $k=0$.

The average scattering per layer which according to Eq. (1) is

$$I_{Av}=\sum_{-\infty}^{+\infty}k\ \tfrac{1}{2}(\mathbf{V}_k\mathbf{V}_0^*+\mathbf{V}_k^*\mathbf{V}_0)$$

is now calculated. Since the phase shift between neighboring layers has been assumed to have a fixed value, φ, $\mathbf{V}_k$ is then given by $\mathbf{V}^{(1)}\exp ik\varphi$ or $\mathbf{V}^{(2)}\exp ik\varphi$ according to whether the kth layer is of the first or second kind and $\mathbf{V}_0$ is simply $\mathbf{V}^{(1)}$ or $\mathbf{V}^{(2)}$. Then the average intensity is

$$I_{Av}=\sum_{-\infty}^{+\infty}k\ \sum_{1}^{r}st\ A_k^{(st)}V^{(s)}V^{(t)}\cos k\varphi.$$

The averaging has been replaced by multiplica-

tion with the probability factors $A_k^{(st)}$ and summation over s and t each of which can assume the values 1 or 2. Using Eq. (22) it follows that

$$I_{\text{av}}=\sum_{-\infty}^{+\infty}k\left[\left(\frac{V^{(1)}+V^{(2)}}{2}\right)^2\cos k\varphi\right]$$

$$+\sum_{-\infty}^{+\infty}k\left[\left(\frac{V^{(1)}-V^{(2)}}{2}\right)^2(4A)^k\cos k\varphi\right].$$

The first term on the right-hand side corresponds to the scattering of a perfectly regular layer lattice in which the layer form factor is $(V^{(1)}+V^{(2)})/2$. The second term gives an intensity

$$I_{\text{cont}}=\left(\frac{V^{(1)}-V^{(2)}}{2}\right)^2\frac{1-(4A)^2}{1-2(4A)\cos\varphi+(4A)^2}. \quad (23)$$

If $A=0$ we have complete disorder and the term reduces to $[(V^{(1)}-V^{(2)})/2]^2$ which is the result found in the first part of the third section. A is positive corresponding to a greater probability of like layers to follow each other. Maxima of intensity occur if $\varphi=n\times 2\pi$, i.e., in the same positions where the regular lattice has its sharp maxima. If A attains its maximum value $\frac{1}{4}$ the crystal breaks up into regions containing exclusively one or the other kind of layer. In this case the second factor in Eq. (23) becomes zero unless φ is $n\times 2\pi$ when both numerator and denominator vanish. For such values of φ the denominator approaches zero quadratically if $(4A)$ approaches unity while the numerator vanishes linearly so that for this ordered case Eq. (23) gives sharp interference maxima the intensities of which are proportional to

$$[(V^{(1)}-V^{(2)})/2]^2.$$

These maxima have the same positions as in an ideal crystal and the sums of the intensities

$$[(V^{(1)}+V^{(2)})/2]^2+[(V^{(1)}-V^{(2)}/2]^2$$

give the average intensity of two crystals with the layer form factors $V^{(1)}$ and $V^{(2)}$.

For negative values of A Eq. (23) has its maxima if φ is an odd multiple of π. This gives half orders lying between the maxima of the regular lattice corresponding to the fact that for negative A values there is a tendency for opposite layers to follow each other. These maxima become sharp for $A=-\frac{1}{4}$ when the random lattice degenerates into a regular superlattice with the layers of the first and second kind alternating.

The most general case is now considered. There shall be r kinds of layers possessing complex scattering vectors $\mathbf{V}^{(1)}, \cdots, \mathbf{V}^{(r)}$ and occurring with frequencies $f^{(1)}, \cdots, f^{(r)}$. The phase shift between two consecutive layers of the s and tth kinds shall be $\varphi^{(st)}$. It will frequently be true that $\varphi^{(st)}=\varphi^{(ts)}$ although this holds necessarily only if the two sides of each layer are equivalent. There also shall be correlations between the probabilities of occurrences of neighboring layers. But the only correlations of probabilities between second and farther neighbors shall be those that follow from correlations of immediate neighbors. An explicit formula for the intensities of scattered x-rays cannot be given. The final formula will contain expressions that depend on solutions of a secular determinant of the rth order.

Denote by $A_1^{(st)}$ the probability that a certain layer shall be of the kind s and the following layer, in a direction considered as positive, of the kind t. The sum

$$\sum_1^r s\,A_1^{(st)}$$

gives the probability that the second layer is of the kind t and therefore must be equal to $f^{(t)}$. One finds in a like manner that

$$\sum_1^r t\,A_1^{(st)}=f^{(s)}.$$

Similarly $A_2^{(st)}$ gives the probability for a layer of the kind s to be followed by a second nearest neighbor of the type t. In general $A_k^{(st)}$ gives the probability that a certain layer is s and that its kth neighbor in the positive direction is t. It again will be frequently true that

$$A_k^{(st)}=A_k^{(ts)}. \quad (24)$$

Also the matrix A_k with the elements $A_k^{(st)}$ is introduced. The matrix is real and if Eq. (24) is satisfied it is symmetrical.

Just as in the special case at the beginning of the section it is useful to introduce numbers $P_k^{(st)}$ which give the probabilities that the kth neighbor of a given layer shall be of the tth kind if the layer itself is of the sth kind. These numbers

are connected with the $A_k^{(st)}$ by the relation

$$A_k^{(st)} = f^{(s)} P_k^{(st)}.$$

Matrices with elements $P_k^{(st)}$ will be represented by P_k. It is then easy to see that the matrix product of P_k and P_1 gives $P_{(k+1)}$ because the probability $P_{(k+1)}{}^{(st)}$ may be written as

$$P_{(k+1)}{}^{(st)} = \sum_1^r q \; P_k{}^{(sq)} P_1{}^{(qt)}.$$

The sum on the right-hand side gives the probabilities of the arrangements of q and t layers in the k and $k+1$ positions if the original layer was of the s kind. And the sum of these probabilities over all possible values of q will give the total probability of s being followed by t as its $(k+1)$th neighbor.

From the above statement about multiplication of P matrices it follows by complete induction that

$$P_k = (P_1)^k$$

The diagonal matrix F with the diagonal elements $f^{(ss)} = f^{(s)}$ is also introduced. Then

$$A_k = FP_k = F(P_1)^k.$$

The average intensity per layer can be written

$$I_{Av} = \sum_{-\infty}^{+\infty} k \sum_1^r st[A_k{}^{(st)} \tfrac{1}{2}(\mathbf{V}_0{}^{(s)} \mathbf{V}_k{}^{(t)*} + \mathbf{V}_0{}^{(s)*} \mathbf{V}_k{}^{(t)})]_{Av}$$

$$= \sum_1^r s \, f^{(s)} \, | \, V_0{}^{(s)} \, |^2 + \sum_1^\infty k \sum_1^r st[A_k{}^{(st)} \mathbf{V}_0{}^{(s)} \mathbf{V}_k{}^{(t)*}]_{Av} + \sum_1^\infty k \sum_1^r st[A_k{}^{(st)} \mathbf{V}_0{}^{(s)*} \mathbf{V}_k{}^{(t)}]_{Av}. \quad (25)$$

The latter expression arises from breaking the sum $\sum_{-\infty}^{+\infty} k$ into a term for $k=0$ and two others for $\sum_1^\infty k$ and $\sum_{-1}^{+\infty} k$. The last two terms in Eq. (25) are conjugate complex and the last can therefore be written $\sum_1^\infty k$ over conjugate complex terms. The scattering vector $\mathbf{V}_0{}^{(s)}$ may be set equal to the layer form factor $\mathbf{V}^{(s)}$ while $\mathbf{V}_k{}^{(t)}$ is the product of the form factor $\mathbf{V}^{(t)}$ and the factor $\exp i\phi_k$. Here $\exp i\phi_k{}^{(st)}$ is the phase shift between the zeroth and kth layers which are of the sth and tth kinds. This phase shift depends of course not only on s and t but also on the kind of the intervening layers. The averaging in Eq. (25) must be carried out over these intervening layers since the averaging over the zeroth and kth layers has already been included explicitly in the summation.

Thus Eq. (25) may be written as

$$I_{Av} = \sum_1^r s \, f^{(s)} \, | \, V_0{}^{(s)} \, |^2 + \sum_1^\infty k \sum_1^r st \mathbf{V}^{(s)} \mathbf{V}^{(t)*} A_k{}^{(st)} [\exp(-i\varphi_k{}^{(st)})]_{Av} + \sum_1^\infty k \sum_1^r st \, \mathbf{V}^{(s)*} \mathbf{V}^{(t)} A_k{}^{(st)} [\exp i\varphi_k{}^{(st)}]_{Av},$$

where the averaging need be carried out only over the exponential factor. This averaging can be carried out by introducing further matrices Q_k with elements $P_k{}^{(st)} \exp(-i\varphi_k{}^{(st)})$. Then the relation holds

$$Q_{(k+1)} = Q_k Q_1. \quad (26)$$

This can be seen in the following way

$$Q_{(k+1)}^{(st)} = P_{(k+1)}^{(st)} [\exp(-i\varphi_{(k+1)}^{(st)})]_{Av} = \sum_1^r q \; P_k{}^{(sq)} P_1{}^{(qt)} \exp(-i(\varphi_k{}^{(sq)} + \varphi^{(qt)})). \quad (27)$$

Indeed $Q^{(st)}{}_{(k+1)}$ is the sum of the phase shifts between layers of s and q kinds occupying the zeroth and kth positions plus the phase shift between two neighboring layers of the qth and tth kinds which have been denoted by $\varphi^{(qt)}$.

Since averaging over q is explicitly included in the summation the averaging process need be

carried out only over the factor $\exp(-i\varphi_k^{(sq)})$ so that Eq. (27) can be written

$$Q_{(k+1)}^{(st)} = \sum_1^r q\, P_k^{(sq)}[\exp(-i\varphi_k^{(sq)})]_{Av} P_1^{(qt)} \exp(-i\varphi^{(qt)}) = \sum_1^r q\, Q_k^{(sq)} Q_1^{(qt)}$$

which proves that Eq. (26) holds.

It follows from Eq. (26) that

$$Q_k = (Q_1)^k. \tag{28}$$

With this notation I_{Av} may be written

$$I_{Av} = \sum_1^r s\, f^{(s)} |V^{(s)}|^2 + \sum_1^\infty k \sum_1^r st\, \mathbf{V}^{(t)*}\mathbf{V}^{(s)} f^{(s)} Q_k^{(st)} + \sum_1^\infty k \sum_1^r st\, \mathbf{V}^{(t)}\mathbf{V}^{(s)*} f^{(s)} Q_k^{(st)*}$$

$$= \sum_1^r s\, f^{(s)} |V^{(s)}|^2 + \sum_1^\infty k \text{ spur } VFQ_k + \sum_1^\infty k \text{ spur } V^*FQ_k^*. \tag{29}$$

Here the symbol spur means the diagonal sum of the matrix product. Matrix Q_k^* is a matrix whose elements are conjugate complexes of the elements of matrix Q_k. The matrices V and V^* have the t, s elements $\mathbf{V}^{(t)*}\mathbf{V}^{(s)}$ and $\mathbf{V}^{(t)}\mathbf{V}^{(s)*}$, respectively.

In order to carry out $\sum_1^\infty k$ it is convenient to transform Q_k to the diagonal form. One can show that this is always possible if one of the two following conditions is satisfied; all proper values of Q_k are different; the matrix A is symmetrical and $\varphi^{(st)} = \varphi^{(ts)}$. (In the latter case the transformation of Q to the diagonal form can be reduced to the transformation of an Hermitian matrix to its diagonal form which can always be carried out.) If none of these conditions holds then it may not be possible to diagonalize Q_k and a formalism is needed that is somewhat more complicated than the one to be presented here.

One may diagonalize the Q matrices by introducing a matrix O for which OQ_1O^{-1} is diagonal. The diagonal elements of this matrix, which are denoted by $Q^{(s)}$, are the solutions of the secular equation belonging to the matrix Q_1. The matrix elements of O may be obtained from a system of homogeneous linear equations whose determinant is the secular equation. The same transformation matrix O that diagonalizes Q_1 also diagonalizes Q_k. This is true because of Eq. (28).

The diagonal elements of OQ_kO^{-1} are the quantities $(Q^{(s)})^k$. The spur occurring in Eq. (29) may now be written as

$$\text{spur } VFQ_k = \text{spur } (OVFO^{-1})(OQ_kO^{-1}).$$

The second factor is in the diagonal form and therefore only the diagonal elements of the first factor enter into the spur. If the first factor is

$$R = OVFO^{-1}$$

whose diagonal elements are $R^{(ss)}$ one obtains for I_{Av}

$$I_{Av} = \sum_1^r s\, f^{(s)} |V^{(s)}|^2 + \sum_1^\infty k \sum_1^r s\, R^{(ss)}(Q^{(s)})^k + \sum_1^\infty k \sum_1^r s\, R^{(ss)*}(Q^{(s)*})^k$$

$$= \sum_1^r s\, f^{(s)} |V^{(s)}|^2 + \sum_1^r s \frac{R^{(ss)}Q^{(s)}}{1-Q^{(s)}} + \sum_1^r s \frac{R^{(ss)*}Q^{(s)*}}{1-Q^{(s)*}}. \tag{30}$$

The first term in this expression represents as usual the average scattering by an isolated layer while the two following terms include the effects due to interferences. Sharp interference maxima may appear when a proper value $Q^{(s)}$ approaches unity provided that the effect is not canceled by the vanishing of the $R^{(ss)}$ value in the numerator.

SECTION 5

The results obtained in the previous section will be now applied to calculate interferences for mica type crystals with an arbitrary amount of randomness in the succession of the layers. It will be

assumed that each layer can occupy one of three positions with equal probability. The positions differ from each other in translations parallel to the plane of the layer by one-third of an identity distance (primitive translation). The distances between neighboring layers are identical so that all phase shifts between neighboring layers may be set equal to a definite quantity φ. The phase shifts due to the translations parallel to the planes of the layers can be incorporated in the layer form factors. All $f^{(s)}$ values are equal to $\frac{1}{3}$.

The layers shall be assumed to be similar on their two faces. Then the most general expression for A_1 consistent with the values of $f^{(s)}$ is

$$A_1=\begin{vmatrix} \frac{1}{3}-(a+b) & a & b \\ a & \frac{1}{3}-(a+c) & c \\ b & c & \frac{1}{3}-(b+c) \end{vmatrix}.$$

The quantities a, b, and c are the probabilities for finding a pair of layers of the kind 1, 2, $\cdots$, 2, 3 or 3, 1, respectively. The probabilities that any layer shall be followed by its own kind can be derived from these numbers.

The matrix Q_1 is given by

$$Q_1=\begin{vmatrix} \frac{1}{3}-(a+b) & a & b \\ a & \frac{1}{3}-(a+c) & c \\ b & c & \frac{1}{3}-(b+c) \end{vmatrix} 3\exp(-i\phi),$$

which symbolizes that each element of the matrix is multiplied by $3\exp(-i\phi)$. The elements of the transformation matrix O may be obtained from the system of linear equations

$$3\exp(-i\varphi)[O^{(s1)}(\tfrac{1}{3}-(a+b))+aO^{(s2)}+bO^{(s3)}]=Q^{(s)}O^{(s1)},$$
$$3\exp(-i\varphi)[aO^{(s1)}+O^{(s2)}(\tfrac{1}{3}-(a+b))+cO^{(s3)}]=Q^{(s)}O^{(s2)},$$
$$3\exp(-i\varphi)[bO^{(s1)}+cO^{(s2)}+O^{(s3)}(\tfrac{1}{3}-(b+c))]=Q^{(s)}O^{(s3)},$$

where $Q^{(s)}$ are proper values of the secular equation

$$\begin{pmatrix} 3[\frac{1}{3}-(a+b)\exp(-i\varphi)]-Q^{(s)}, & 3a\exp(-i\varphi), & 3b\exp(-i\varphi) \\ 3a\exp(-i\varphi), & 3[\frac{1}{3}-(a+c)\exp(-i\varphi)]-Q^{s}, & 3c\exp(-i\varphi) \\ 3b\exp(-i\varphi), & 3c\exp(-i\varphi), & 3[\frac{1}{3}-(b+c)\exp(-i\varphi)]-Q^{s} \end{pmatrix}=0.$$

One finds the three proper values

$$Q^{(1)}=\exp(-i\varphi),$$
$$Q^{(2)}=[1-3(a+b+c)+3M^{\frac{1}{2}}]\exp(-i\varphi),$$
$$Q^{(3)}=[1-3(a+b+c)-3M^{\frac{1}{2}}]\exp(-i\varphi),$$

where $M=[a^2+b^2+c^2-ab-bc-ca]$ while for the matrix O one finds

$$O=\begin{vmatrix} 1/\sqrt{3} & 1/\sqrt{3} & 1/\sqrt{3} \\ 1/\sqrt{6}[1-\Lambda] & 1/\sqrt{6}[\epsilon+\Lambda\epsilon^*] & 1/\sqrt{6}[\epsilon^*+\Lambda\epsilon] \\ 1/\sqrt{6}[1+\Lambda] & 1/\sqrt{6}[\epsilon-\Lambda\epsilon^*] & 1/\sqrt{6}[\epsilon^*-\Lambda\epsilon] \end{vmatrix}.$$

Here the following abbreviations have been used

$$\epsilon=\exp(2\pi i/3),\quad \epsilon^*=\exp(-2\pi i/3),$$
$$\Lambda=(a\epsilon+b\epsilon^*+c)M^{-\frac{1}{2}}.$$

The matrix O^{-1} may be obtained from O by interchanging rows and columns and taking conjugate complex values.

The matrix F is simply

$$F=\begin{vmatrix} \frac{1}{3} & O & O \\ O & \frac{1}{3} & O \\ O & O & \frac{1}{3} \end{vmatrix}.$$

Since the three kinds of layers differ only in translations the absolute layers of the layer form factors are all equal and can be denoted by V. Corresponding to the translations by $\frac{1}{3}$ primitive distance the layer form factors will differ by complex cube roots of unity and the V matrix can be written as

$$V=\begin{vmatrix} V^2 & \epsilon V^2 & \epsilon^* V^2 \\ \epsilon^* V^2 & V^2 & \epsilon V^2 \\ \epsilon V^2 & \epsilon^* V^2 & V^2 \end{vmatrix}.$$

Taking the diagonal elements of the matrix $OVFO^{-1}$ one obtains

$$R^{(11)}=0, \quad R^{(23)}=R^{(33)}=\tfrac{1}{2}V^2.$$

Thus the expression for the average intensity is

$$\frac{2I_{Av}}{V^2}=2+\frac{[1-3(a+b+c)+3M^{\frac{1}{2}}]\exp(-i\varphi)}{1-[1-3(a+b+c)+3M^{\frac{1}{2}}]\exp(-i\varphi)}+\frac{[1-3(a+b+c)-3M^{\frac{1}{2}}]\exp(-i\varphi)}{1-[1-3(a+b+c)-3M^{\frac{1}{2}}]\exp(-i\varphi)}+\text{conjugate complex},$$

$$I_{Av}=V^2\left[\frac{(1-D)(1+D-F\cos\varphi)}{1+F^2+D^2-2F(1+D)\cos\varphi+2D\cos 2\varphi}\right], \tag{31}$$

where the quantities F and D are defined by

$$F=2-6(a+b+c),$$
$$D=1-6(a+b+c)+27(ab+ac+bc).$$

For the case of complete order $a=b=c=0$, which leads to $F=2$, $D=1$. Then the numerator of Eq. (31) vanishes and there is no scattering except where $\varphi=n\times 2\pi$ in which case the denominator of Eq. (31) is also zero. By assuming small but not vanishing values for a, b, and c it can be shown that intensity maxima occur for $\varphi=n\times 2\pi$ and these maxima go toward infinity when a, b, and c go toward zero.

The case of complete disorder is obtained for $a=b=c=\frac{1}{9}$. For this case the matrix A_1 shows that any sequence of two layers is equally probable. For this case $F=D=0$ and the intensity becomes equal to V^2 independently of φ as should be indeed expected from the discussion given in the beginning of Section 3.

A third extreme case is obtained by setting $a=b=c=\frac{1}{6}$. This is the maximum value that the three quantities can attain if they are equal to each other. It physically corresponds to the situation where a layer can be followed with equal probability by either of the other two layers but not by itself. Then we have $F=-1$, $D=\frac{1}{4}$. The average intensity becomes

$$I_{Av}=V^2\left[\frac{15+12\cos\varphi}{33+40\cos\varphi+8\cos 2\varphi}\right].$$

This function has relatively broad maxima when φ is an odd multiple of π and minima when $\varphi=n\times 2\pi$. The intensity in the minima is $\frac{1}{9}$ of

the maxima. It is none too surprising that we now obtain minima where for an ordered lattice sharp maxima would occur since the scattering phases of neighboring layers are shifted 120° compared with the scattering of layers in an ordered structure.

A simple example in which a, b, and c are not equal is furnished by $a=\frac{1}{6}$, $b=c=0$ which gives $F=1$, $D=0$.

$$I_{Av}=V^2(1-\cos\varphi)/(2-2\cos\varphi).$$

This gives $V^2/2$ whenever $\varphi\neq n\times 2\pi$. If $\varphi=n\times 2\pi$ the expression becomes indeterminate. Assuming small but not vanishing values for b and c it can be shown that sharp intensity maxima occur for such values of φ. The case discussed at present corresponds to a crystal broken up into two kinds of regions, first into a random mixture of the 1st and 2nd kind of layer and second into an ordered structure of the 3rd kind of layer. The intensity function gives a structureless continuum with sharp interference maxima superimposed upon it. It must be noticed, however, that the sharp maxima are only partly due to the ordered portions of the crystals while they partly are caused by the fact that in the random parts of the crystal the average value of the scattering power is different from zero.

It is of interest to notice that while the correlation probabilities are described by three parameters a, b, and c, only two combinations of these parameters F and D enter into the intensity distribution.

From the cases discussed above the effect of the two parameters F and D becomes apparent. According to their different values interference maxima may become sharper or broader and also the background may have various intensities. But as shown by the last example there is no unique relationship between breadth of maxima and intensity of the background. A background may appear even if the maxima are quite sharp.

SECTION 6

In the last example that is to be treated correlations are assumed between layers that are second neighbors so that the treatment of the previous section is not directly applicable. However, by the artifice of considering pairs of layer as forming, one layer of this case can be reduced to the one for which the general treatment has been given.

A physical realization of the arrangement of layers that will be considered is a close packed structure of spheres in which the layers in question are the most densely packed arrangement of spheres. One of these, namely the cubic packed arrangement, can be represented by successive layers which are displaced with regard to each other by a translation perpendicular to the plane and by $\frac{1}{3}$ of a certain primitive translation parallel to the plane. The three different positions obtainable by the latter translation will be designated by I, II, and III and the cubic arrangement is characterized by the sequence $\cdots$I, II, III, I, II, III, I$\cdots$ or equally by $\cdots$I, III, II, I, III, II, I$\cdots$.

The second well-known close packing of spheres is the hexagonal close packed structure which can be described by either one of the three sequences

$$\cdots\text{I, II, I, II, I, II}\cdots$$
$$\cdots\text{II, III, II, III, II, III}\cdots$$
$$\cdots\text{III, I, III, I, III, I}\cdots$$

In these structures a layer is always followed by a layer of a different kind and as far as interaction between neighbors is concerned there is equal likelihood of a layer being followed by either one of the two remaining kinds of layers. The cubic and hexagonal structures differ in so far that in the cubic structure second neighboring layers must also be of a different kind while in the hexagonal arrangement second neighbors are of the same kind. Arrangements will now be discussed having certain degrees of randomness in which first neighbors are always different but second neighbors have certain probabilities to be alike or unlike.[7]

A second physical realization of the sequence of layers to be discussed is afforded by graphite crystals. The layers of carbon atoms have an arrangement as shown in Fig. 2. Successive layers are shifted parallel to the planes of layers by one-third of the primitive translation. In the graphite structure as described one finds an

[7] O. S. Edwards, H. Lipson, and A. J. C. Wilson, Nature **148**, 165 (August 9, 1941) have observed structures involving mixtures of hexagonal and cubic close packing in metallic cobalt.

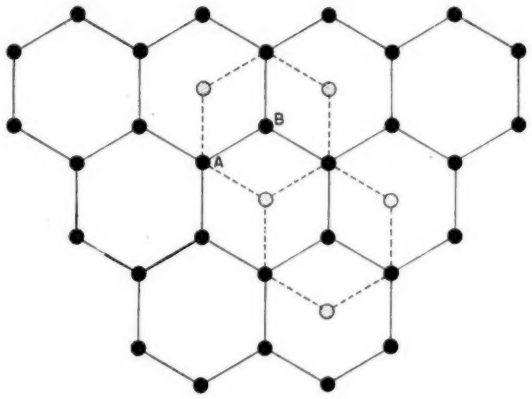

FIG. 2. Atomic arrangement in a carbon layer of graphite. Atoms in adjacent layers can either be above A or B, but only above one of them in an ordered crystal.

ordered sequence in which every second layer is alike. Since in other samples of graphite completely random shifts along the planes of the layers have been observed it is conceivable that crystals can be found in which the normal $\frac{1}{3}$ primitive translation between layers is strictly preserved while an arbitrary correlation exists between translations of second layers.

In order to reduce formulas to one with correlations between neighboring layers pairs of layers are considered as units. Six pairs can exist

(I, II)(II, III)(III, I)(II, I)(III, II)(I, III)

each of which occurs with the frequency $\frac{1}{6}$. First consider by what kinds of layers (I, II) can be followed. According to the above statements the sequences (I, II), (II, III) and (I, II)(II, I) cannot occur. It is assumed that the frequencies with which the combinations (I, II)(I, II), (I, II)(I, III), and (I, II)(III, I) occur are in the ratio $1:x:y$. The combination (I, II)(III, II) has the same frequency as (I, II)(I, III). In fact the probabilities remain unchanged if the designations I, II, and III are permuted in any way or if sequences are read in the opposite directions, since the original restrictions relate only to the questions of similarity or dissimilarity of first and second neighbors. Now the sequence (I, II)(I, III) can be turned into the sequence (I, II)(III, II) by substituting I for III, II for I, III for II and reading in the reverse direction. By similar methods one can obtain all other sequences from those mentioned above.

A connection between the relative proabilities x and y can be established if it is recalled that the grouping of the layers I, II, and III into pairs was arbitrary. Consider the question of the probability with which a layer I will be followed by the same kind of layer in the third place. There are two ways in which this can happen; namely, by the arrangement (I, II)(III, I) or by (I, III)(II, I). Assuming that the first layer is of the kind I the probability that the first pair of layers is (I, II) will be $\frac{1}{2}$. This pair can be followed by the combination (I, II), (I, III)(III, II) $\times$(III, I) with the relative probabilities 1, x, x, and y. Therefore the probability for the sequence (I, II)(III, I) is $\frac{1}{2}[y/(1+2x+y)]$ supposing that the first layer was of the kind I. By a similar argument it can be shown that the sequence (I, III)(II, I) has the same probability so that the total probability of I being followed in the third place by I is $y/(1+2x+y)$.

The same probability may be calculated also in a somewhat more complicated manner by adding the probabilities of occurrences for the following eight combinations

$$
\begin{aligned}
&(\text{II}, I)(\text{II}, \text{III})(\text{I}, \text{III}) && \frac{1}{2}\ \frac{x}{1+2x+y}\ \frac{x}{1+2x+y}\\
&(\text{II}, I)(\text{II}, \text{III})(\text{I}, \text{II}) && \frac{1}{2}\ \frac{x}{1+2x+y}\ \frac{y}{1+2x+y}\\
&(\text{II}, I)(\text{III}, \text{II})(\text{I}, \text{II}) && \frac{1}{2}\ \frac{x}{1+2x+y}\ \frac{x}{1+2x+y}\\
&(\text{II}, I)(\text{III}, \text{II})(\text{I}, \text{III}) && \frac{1}{2}\ \frac{y}{1+2x+y}\ \frac{y}{1+2x+y}
\end{aligned}
$$

and four more combinations in which layers two and three are systematically replaced by each other. The probabilities of these combinations are indicated after the symbols assuming that the italicized layer is of the kind I. These four probabilities have to be added and multiplied by two to take into account combinations in which II and III are interchanged. One obtains $[(x+y)/(1+2x+y)]^2$ for the same probability for which $y/(1+2x+y)$ was obtained above. These two quantities can be equal only if $y=x^2$. Thus all probabilities can be reduced to the relative probabilities $1 : x$ for the sequences (I, II)(I, III) and (I, II)(I, III).

Taking into account the relative probability of sequences and the frequencies for individual pairs one obtains for the A matrix

$$A=\begin{array}{r|cccccc|}
 & \text{I, II} & \text{II, III} & \text{III, I} & \text{II, I} & \text{III, II} & \text{I, III} \\
\text{I, II} & 1 & 0 & X^2 & 0 & X & X \\
\text{II, III} & X^2 & 1 & 0 & X & 0 & X \\
\text{III, I} & 0 & X^2 & 1 & X & X & 0 \\
\text{II, I} & 0 & X & X & 1 & X^2 & 0 \\
\text{III, II} & X & 0 & X & 0 & 1 & X^2 \\
\text{I, III} & X & X & 0 & X^2 & 0 & 0
\end{array}\Bigg|\frac{1}{6(X+1)^2},$$

where it is indicated that each element of the matrix is to be multiplied by $1/6(X+1)^2$. In the above form it has been indicated to which pair of layers each row and column corresponds. It will be observed that A is not symmetrical.

The phase shifts between consecutive pairs of layers may be written as the same number φ for any sequence. The effect of shifts parallel to the layers may be included in the complex layer form factors V. The matrix Q_1 then becomes

$$Q_1=\frac{\exp(-i\varphi)}{(1+X)^2}\begin{vmatrix}
1 & 0 & X^2 & 0 & X & X \\
X^2 & 1 & 0 & X & 0 & X \\
0 & X^2 & 1 & X & X & 0 \\
0 & X & X & 1 & X^2 & 0 \\
X & 0 & X & 0 & 1 & X^2 \\
X & X & 0 & X^2 & 0 & 1
\end{vmatrix}$$

where $\exp(-i\varphi)/(1+X)^2$ written before the matrix indicates that each element of the matrix contains this as a factor.

This matrix can be diagonalized by means of the matrix

$$O=\frac{1}{\sqrt{6}}\begin{vmatrix}
1 & 1 & 1 & 1 & 1 & 1 \\
1 & 1 & 1 & -1 & -1 & -1 \\
1 & \epsilon & \epsilon^* & [\alpha^+] & [\alpha^+]\epsilon & [\alpha^+]\epsilon^* \\
1 & \epsilon^* & \epsilon & [\alpha^+]^* & [\alpha^+]^*\epsilon^* & [\alpha^+]^*\epsilon \\
1 & \epsilon & \epsilon^* & [\alpha^-] & [\alpha^-]\epsilon & [\alpha]\epsilon^* \\
1 & \epsilon^* & \epsilon & [\alpha^-]^* & [\alpha^-]^*\epsilon^* & [\alpha^-]^*\epsilon
\end{vmatrix}$$

and by the reciprocal matrix O^{-1}.

The symbols ϵ and ϵ^* have the same meaning as in the first part of the section and the abbreviations

$$\alpha^+ = \frac{x+(4-3x^2)^{\frac{1}{2}}}{2}+\epsilon x,$$

$$\alpha^- = \frac{x-(4-3x^2)^{\frac{1}{2}}}{2}+\epsilon x.$$

Their conjugate complex values are indicated by asterisks. With the transformation OQ_1O^{-1} the proper values of Q_1 are

$$Q^{(1)} = \exp(-i\varphi),$$

$$Q^{(2)} = \left(\frac{x-1}{x+1}\right)^2 \exp(-i\varphi),$$

$$Q^{(3)} = Q^{(4)} = \left[\frac{1-[\alpha^+]x+\epsilon x^2}{(1+x)^2}\right] \exp(-i\varphi),$$

$$Q^{(5)} = Q^{(6)} = \left[\frac{1-[\alpha^-]x+\epsilon x^2}{(1+x)^2}\right] \exp(-i\varphi).$$

It will be noticed that the matrix Q_1 could be diagonalized in spite of the fact that A is not symmetrical and all the proper values of Q are not different. Actually the fulfillment of one of these conditions as given in Section 4 is a sufficient but not necessary condition for transforming Q_1 to a diagonal matrix.

The matrix F is a diagonal matrix with all diagonal elements equal to $\frac{1}{6}$. The matrix V may be written after taking into account the translation by $\frac{1}{3}$ and $\frac{2}{3}$ the primitive translations in layers of type II and III

$$V = 2|V|^2 \begin{vmatrix} T^+ & \epsilon T^+ & \epsilon T^+ & T & \epsilon T & \epsilon^* T \\ \epsilon^* T^+ & T^+ & \epsilon T^+ & \epsilon^* T & T & \epsilon T \\ \epsilon T^+ & \epsilon^* T^+ & T^+ & \epsilon T & \epsilon^* T & T \\ T & \epsilon T & \epsilon^* T & T^- & \epsilon T^- & \epsilon^* T^- \\ \epsilon^* T & T & \epsilon T & \epsilon^* T^- & T^- & \epsilon T^- \\ \epsilon T & \epsilon^* T & T & T^- & \epsilon^* T^- & T^- \end{vmatrix}$$

where the abbreviations

$$T = -\tfrac{1}{2}+\cos\varphi/2,$$

$$T^+ = 1+\cos(\varphi/2+2\pi/3),$$

$$T^- = 1+\cos(\varphi/2-2\pi/3)$$

have been used. The quantity $|V|^2$ is the square of the absolute value of the layer form factor for a layer of the type I, II, or III.

Calculating the diagonal elements of the matrix

$$R = OVFO^{-1}$$

one obtains

$$R^{(11)} = R^{(22)} = R^{(44)} = R^{(66)} = 0,$$

$$R^{(33)} = -\frac{[\alpha^-]T^+ + [\alpha^+]T^- + 2T}{[\alpha^+]-[\alpha^-]},$$

$$R^{(55)} = \frac{[\alpha^+]T^+ - [\alpha^-]T^- - 2T}{[\alpha^+]-[\alpha^-]}.$$

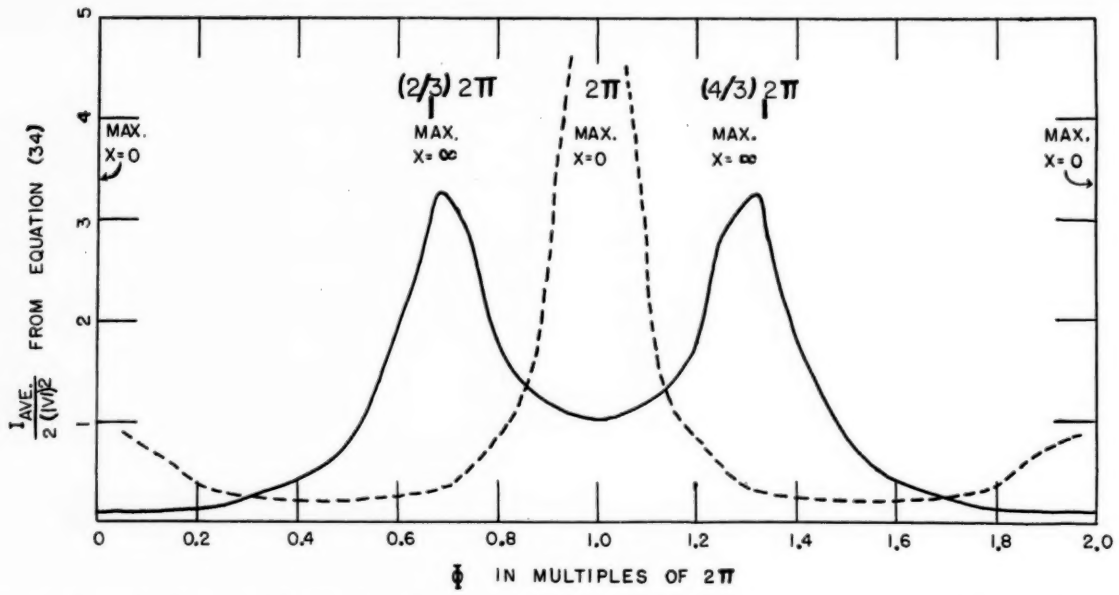

FIG. 3. Scattering from mixed cubic ($x=\infty$) and hexagonal ($x=0$) close packed structures. The solid curve gives the value of expression (34) for $x=3.0$ and the dotted curve for $x=0.3$.

Substituting these quantities into Eq. (30) the average intensity per layer is found to be

$$\frac{I_{Av}}{|V|^2}=\frac{(-[\alpha^-]T^+ +[\alpha^+]T^- +2T)(1-[\alpha^+]x+\epsilon x^2)\exp(-i\varphi)}{([\alpha^+]-[\alpha^-])[(1+x)^2-(1-[\alpha^+]x+\epsilon x^2)\exp(-i\varphi)]}$$

$$+\frac{([\alpha^+]T^+ -[\alpha^-]T^- -2T)(1-[\alpha^-]x+\epsilon x^2)\exp(-i\varphi)}{([\alpha^+]-[\alpha^-])[(1+x)^2-(1-[\alpha^-]x+\epsilon x^2)\exp(-i\varphi)]}+\text{conjugate complex}+(T^+ +T^-). \quad (32)$$

The last term in Eq. (32) gives the average scattering of an isolated layer. Equation (32) can be expressed in the somewhat simpler form

$$\frac{I_{Av}}{|V|^2}=\frac{(1+x)^2}{[\alpha^+]-[\alpha^-]}\left[\frac{-[\alpha^-]T^+ +[\alpha^+]T^- +2T}{(1+x)^2-[1-[\alpha^+]x+\epsilon x^2]\exp(-i\varphi)}\right.$$

$$\left.+\frac{+[\alpha^+]T^+ -[\alpha^-]T^- -2T}{(1+x)^2-[1-[\alpha^-]x+\epsilon x^2]\exp(-i\varphi)}\right]+\text{conjugate complex}-(2-\cos\varphi/2). \quad (33)$$

Substituting into Eq. (33) the values of $[\alpha^+]$, $[\alpha^-]$, $[T^+]$, and T^- one finally obtains

$$\frac{I_{Av}}{|V|^2}=\frac{(1+x)^2}{(4-3x^2)^{\frac{1}{2}}}\left[\frac{(4-3x^2)^{\frac{1}{2}}(2-\cos\varphi/2)+3ix\sin\varphi/2-2+4\cos\varphi/2}{2(1+x)^2-(2-x^2-x(4-3x^2)^{\frac{1}{2}})\exp(-i\varphi)}\right.$$

$$\left.+\frac{(4-3x^2)^{\frac{1}{2}}(2-\cos\varphi/2)-3ix\sin\varphi/2+2-4\cos\varphi/2}{2(1+x)^2-(2-x^2+x(4-3x^2)^{\frac{1}{2}})\exp(-i\varphi)}\right]+\text{conjugate complex}-(2-\cos\varphi/2). \quad (34)$$

The limiting case of hexagonal close packing is obtained for $x=0$. Substitution in (34) shows that I_{Av} indeed vanishes for $x=0$ and $\exp(i\varphi)\neq 1$. Now $\exp(i\varphi)=1$ is just the interference condition for a hexagonal lattice since φ was the phase shift between second neighbors and this is the identity

distance in the hexagonal packing. For $\exp(i\varphi)=1$ and $x=0$ Eq. (34) becomes indeterminate. By carrying out the process $x\rightarrow 0$ one obtains intensity maxima in the correct position that approach infinity as $1/x$.

The other limiting condition $x=\infty$ corresponds to a cubic close packed arrangement. In this case Eq. (34) vanishes except when φ is an integral multiple of $4\pi/3$ but not of 2π. Indeed if second neighbors have such phase shifts the phase shift of third neighbors becomes a multiple of 2π. For cubic close packing the distance of third neighbors is the primitive distance. If φ is a multiple of $4\pi/3$ but not of 2π and if $x\rightarrow\infty$ Eq. (34) approaches ∞ proportional to x and we again obtain sharp interference maxima. These maxima may be interpreted as belonging to a mixture of two cubic close packed crystals; one with the sequence of layers $\cdots$I II III I II III$\cdots$ gives interference maxima at $\varphi=-4\pi/3+n\times 2\pi$ (n is $+$ $-$ or 0); the sequence of layers $\cdots$I III II I III II$\cdots$ gives maxima at $\varphi=4\pi/3+n\times 2\pi$.

It can be seen from the form of Eq. (34) that for values of x between zero and infinity no sharp maxima occur and indeed these intermediate values correspond to imperfectly ordered arrangements. Values of Eq. (34) calculated for $x=0.3$ and $x=3.0$ are shown in Fig. 3. Positions of interference maxima for the ordered systems having $x=0$ and $x=\infty$ are also indicated.

MARCH, 1942 JOURNAL OF CHEMICAL PHYSICS VOLUME 10

Supersonic Measurement of the Heat Capacity of Propylene

D. TELFAIR*
Department of Physics, The Pennsylvania State College, State College, Pennsylvania
(Received November 22, 1941)

An apparatus designed for (1) a general study of acoustical dispersion in gases, and (2) measurement of gaseous heat capacities has been used to measure the heat capacity of propylene between 273 and 490°K. The general methods used are outlined and discussed. The measured heat capacity values agree well with those calculated from the frequency assignment as given by Wilson and Wells, and an assumed potential restricting rotation of about 2000 cal./mole, but deviate from the values calculated from Pitzer's frequency assignment and an 800-cal./mole potential. The measurements on propylene also have the value of serving as a test of the usefulness and practicality of the supersonic method of heat capacity determinations.

INTRODUCTION

VARIOUS workers have used sound velocity measurements as a means of determining gaseous heat capacities.[1-7] For some time this was considered as one of the most precise and reliable methods. The discovery and subsequent investigation of intramolecular dispersion, however, made it apparent that sonic methods might yield misleading results, since the presence of lagging vibrational states is accompanied by an abnormally high velocity unless the frequency used is low enough to allow all modes of storing energy to stay in equilibrium with the fluctuating pressure and temperature which accompany the passage of a sound wave through a gas.

The development of the Pierce acoustic interferometer[8] put into the hands of the experimenter an instrument capable of very precise velocity determinations, but only a few attempts have been made to use it for heat

* Now with the Plastics Division of the Monsanto Chemical Company at Springfield, Massachusetts.

[1] Kundt, Pogg. Ann. **135**, 337 (1868).
[2] Wullner, Ann. d. Physik **4**, 321 (1878).
[3] Capstick, Phil. Trans. Roy. Soc., **185**, 1 (1895).
[4] E. H. Stevens, Ann. d. Physik **7**, 285 (1902).
[5] Kalahne, Ann. d. Physik **11**, 225 (1903).
[6] Dixon, Campbell, and Parker, Proc. Roy. Soc. **100**, 1 (1922).
[7] J. R. Partington and W. C. Shilling, Phil. Mag. **3**, 273 (1927); Phil. Mag. **6**, 920 (1928).
[8] G. W. Pierce, Proc. Am. Acad. Arts and Sci. **60**, 271 (1925).

capacity measurements[9–13] principally for the reason outlined above.

However, it seems probable that the sonic method of heat capacity determinations can still be used in many cases, especially when viewed in the light of recent work by Eucken and his co-workers.[14,15] The latter have pointed out that for all polyatomic gases examined so far, one obtains a single smooth dispersion curve similar to that for the simple case of an idealized gas with only one vibrational quantum state above the ground state. Thus, gases behave as if all of the vibrational quantum transitions have the same (or nearly the same) relaxation time. By locating the corresponding single dispersive region with preliminary velocity and absorption measurements, one may frequently choose the conditions of measurement (temperature, pressure, and frequency), in such a way as to be on the normal, low frequency, low velocity side of the dispersive region, and consequently measure a velocity corresponding to the true, or total heat capacity. The application of this method to gaseous propylene is described below.

METHODS USED

The apparatus used will be described in detail in another journal.† Briefly, it consists of a Pierce acoustic interferometer which, in general design and purpose is similar to the one described by Eucken and Nümann.[16] The interferometer chamber, which may be evacuated, is operated in conjunction with a temperature control system, a vacuum system, and a potentiometer for temperature measurement. The half-wave-length spacings are accurately determined with a calibrated micrometer screw, and the frequency of the quartz crystal source is determined with high precision by measuring the audible beat note obtained with an ordinary broadcast receiver when the radiofrequency signal from the crystal is picked up together with a broadcast carrier signal of frequency close to that of the crystal. The velocity is then obtained from the product of the wave-length and the frequency.

The absorption is calculated from plate current readings taken simultaneously with the micrometer screw readings which are used in calculating the velocity. The peak and trough values of the plate current are recorded for each setting of the micrometer screw, and the absorption is calculated from the logarithmic decrement of these peak-to-trough differences of the plate current, as the reflector is moved away from the crystal. This method has been justified experimentally by Pielemeier[17] and van Itterbeek[18] and has been given a much more satisfactory theoretical basis by Hardy,[19] who has demonstrated that it gives a good approximation to the true absorption, provided a small amplitude source and path differences far from the source are used. These conditions were satisfied for the measurements reported below.

The velocity of propagation of plane sound waves in any fluid is given with sufficient exactness for all practical cases by the equation

$$V^2=\gamma\frac{E_i}{\rho}=-\frac{C_p}{C_v}\frac{v}{\rho}\left(\frac{\partial p}{\partial v}\right)_T, \tag{1}$$

where γ = the heat capacity ratio, C_p/C_v,
E_i = the isothermal elasticity,
ρ = the density,
p = the pressure,
v = the volume.

The equation of state may be used (a) to evaluate the isothermal elasticity, $-v(\partial p/\partial v)_T$, and (b) to express C_p in terms of C_v. Thus, for a perfect gas, a useful form of Eq. (1) becomes

$$V^2=(RT/M)(1+R/C_v), \tag{2}$$

where R = the gas constant per mole,
M = molecular weight,
T = the absolute temperature.

[9] W. C. Shilling and J. R. Partington, Phil. Mag. **9**, 1020 (1930).
[10] A. Eucken and R. Becker, Zeits. f. physik. Chemie **B27**, 235 (1934).
[11] R. Schultze, Ann. d. Physik **34**, 41 (1939).
[12] S. K. K. Jatkar, Ind. J. Phys. **13**, 445 (1939).
[13] Van Lammeran, Physica **2**, 833 (1935).
[14] A. Eucken and S. Aybar, Zeits. f. physik. Chemie **B46**, 195 (1940).
[15] K. Schafer, Zeits. f. physik. Chemie **B46**, 212 (1940).
† D. Telfair and W. H. Pielemeier, Rev. Sci. Inst., in press.
[16] A. Eucken and E. Nümann, Zeits. f. physik. Chemie **B36**, 163 (1937).
[17] W. H. Pielemeier, Phys. Rev. **34**, 1184 (1929).
[18] A. van Itterbeek and P. Mariëns, Physica **4**, 207 (1937).
[19] H. C. Hardy, Doctor's Thesis, Pennsylvania State College (1941) (to be published soon).

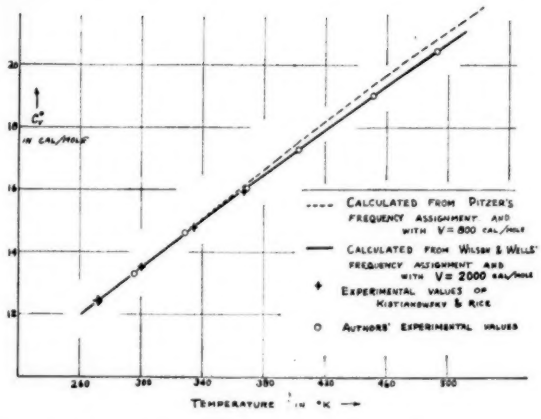
C_v
IN CAL/MOLE
CALCULATED FROM PITZER'S FREQUENCY ASSIGNMENT AND WITH V= 800 CAL/MOLE
CALCULATED FROM WILSON & WELLS' FREQUENCY ASSIGNMENT AND WITH V= 2000 CAL/MOLE
EXPERIMENTAL VALUES OF KISTIAKOWSKY & RICE
AUTHORS' EXPERIMENTAL VALUES
TEMPERATURE IN °K

FIG. 1. Measured and calculated values of the constant volume molal heat capacity of propylene.

This same useful form may be retained for real gases. By assuming an equation of state of the form

$$pv = RT + \beta/v + \delta/v^2 + \epsilon/v^3 + \cdots, \quad (3)$$

Hardy[20] has carried through a rigorous derivation of the equation

$$V^2 = (RT/M)(P + QR/C_v). \quad (4)$$

The quantities

$$P = 1 + 2\beta/RTv + 3\delta/(RTv^2) + \cdots \quad (5)$$

and

$$Q = \left[1 + \frac{1}{Rv}\left(\frac{\partial\beta}{\partial T}\right)_v + \frac{1}{Rv^2}\left(\frac{\partial\delta}{\partial T}\right)_v + \cdots\right]^2 \quad (6)$$

are dimensionless and approach unity as the gas approaches perfection. Thus, if the velocity has been measured, the molal heat capacity at constant volume may be obtained from Eq. (4). By solving for C_v we obtain

$$C_v = \frac{QR}{(V^2M/RT - P)}. \quad (7)$$

Finally, using the value of C_v calculated by means of Eq. (7), we obtain C_v^0, the constant volume molal heat capacity for an infinitely dilute gas, from the familiar thermodynamic expression

$$C_v^0 = C_v - \int_\infty^v T\left(\frac{\partial^2 p}{\partial T^2}\right)_v dv, \quad (8)$$

which, using (3) as the equation of state, becomes

$$C_v^0 = C_v + \frac{T}{v}\left[\left(\frac{\partial^2\beta}{\partial T^2}\right)_v + \frac{1}{2v}\left(\frac{\partial^2\delta}{\partial T^2}\right)_v + \cdots\right]. \quad (9)$$

If absorption measurements are made simultaneously with velocity measurements, a consideration of the way in which the absorption changes with frequency and/or gas density will show on which side of the dispersive region these measurements lie. Also, the numerical value of the absorption allows one to estimate quantitatively how far the measurements are removed from the dispersive region.

THE HEAT CAPACITY OF PROPYLENE

The propylene used in these measurements was furnished by the Pennsylvania State College Cryogenic Laboratory. Vapor pressure readings taken during its purification indicated that the impurity was not greater than 0.05 percent.

Preliminary measurements of velocity and absorption taken at various frequencies, pressures, and temperatures show that even for 0°C and 1.2 megacycles, propylene is well on the normal low frequency, low velocity side of the dispersive region. The absorption, measured as described above, is very nearly as low for propylene at all the temperatures at which measurements were taken, as it is at room temperature for air, or nitrogen, which have very little intramolecular absorption. Consequently, propylene, under these conditions, must be far removed from any dispersive regions. By making use of (1) the measured absorption, (2) the fact that the absorption increases with frequency, and (3) the expression which gives μ, the absorption per wave-length, as a function of the frequency,[21] it is possible to calculate an approximate value for the frequency at which maximum absorption would occur in propylene. If based on the reasonable assumption that all modes of vibration in propylene have the same relaxation time, such a calculation indicates that the frequency for maximum absorption would occur between 80 and 100 megacycles. This corresponds to a relaxation time of approximately 10^{-8} second.

[20] H. C. Hardy, Paper No. 1, Rochester Meeting of the Acoustical Society of America, May 5–7, 1941.

[21] W. H. Pielemeier, H. L. Saxton and D. Telfair, J. Chem. Phys. **8**, 106 (1940).

From these considerations we may conclude that either (a) all of the quantum vibrational states of propylene, under the conditions of our measurements, have such a short mean quantum lifetime that they are able to stay in equilibrium with the rapid pressure and temperature fluctuations of the sound wave, or (b) only states corresponding to high wave numbers, and therefore contributing only slightly to the total heat capacity, have "dropped out" of the acoustical cycle at much lower frequencies. (If states of low wave numbers had "dropped out" at lower frequencies, the absorption would, of necessity, decrease with an increase in log (f/p), whereas it is observed to increase.)

As evidence that (a) actually obtains rather than (b), we present the close agreement between the values of C_v^0 (the constant volume molal heat capacity for infinite dilution) as calculated from velocity measurements with those determined by Kistiakowsky and Rice[22] by an independent method (see Fig. 1).

Berthelot's equation of state was first used for the C_v^0 calculations but was found to be entirely inadequate. Fortunately, the second virial coefficient β has been determined for propylene experimentally. We have used the value given by Roper[23] in order to calculate C_v^0 for each of the seven temperatures indicated in Fig. 1. Since small ranges of pressure were used (from $\frac{1}{4}$ to 2 atmos.), the second virial coefficient only was considered as sufficient for our calculations.

In order to present the results in a more convenient form, the C_v^0 values as read from a larger scale plot of Fig. 1 for temperature intervals of ten degrees lying between 270 and 510°C have been listed in Table I.

THE RESTRICTED ROTATION POTENTIAL AND FREQUENCY ASSIGNMENT IN PROPYLENE

As recently pointed out,[24] a potential restricting rotation of the methyl group in propylene of about 800 cal./mole, and the fundamental vibrational frequencies as assigned by Pitzer[25] do not disagree with the measured heat capacity of propylene between 273 and 367°K as reported by Kistiakowsky and Rice.[22] However, the set of frequencies recently assigned by Wilson and Wells,[26] and a potential restricting rotation of about 2000 cal./mole are also in agreement with the measured values of the heat capacity. By extending the heat capacity measurements to higher temperatures we have made possible a choice between the two assignments. As shown in Fig. 1 the measured heat capacities at the higher temperatures (between 360 and 500°K) are still in excellent agreement with values calculated from the Wilson-Wells assignment and a 2000-cal./mole potential, but values calculated from Pitzer's assignment and an 800-cal./mole potential deviate by considerably more than the limits of accuracy of the measurements. In these calculations we have used Pitzer's tables[27] for the heat capacity of a restricted rotator. Pitzer and Gwinn[28] have recently shown that these tables are applicable to a molecule like propylene, which consists essentially of a rigid frame with an attached symmetrical top whose rotation is hindered.

TABLE I. Constant volume molal heat capacities of propylene for an infinitely dilute gas.

Temperature	C_v^0 cal/mole	Temperature	C_v^0 cal/mole
270°K	12.30	400°K	17.17
280	12.70	410	17.53
290	13.09	420	17.89
300	13.48	430	18.24
310	13.86	440	18.59
320	14.24	450	18.94
330	14.62	460	19.29
340	14.99	470	19.63
350	15.36	480	19.98
360	15.73	490	20.32
370	16.09	500	20.66
380	16.45	510	21.00
390	16.81		

Attention is called to the fact that the slope of the Wilson-Wells curve is everywhere in agreement with the slope for the measured values of the C_v^0 curve, whereas the Pitzer curve is not. Thus, Pitzer's frequency assignment with a potential barrier lower than 800 cal./mole might

[22] G. B. Kistiakowsky and W. W. Rice, J. Chem. Phys. **8**, 610 (1940).
[23] E. E. Roper, J. Phys. Chem. **44**, 835 (1940).
[24] D. Telfair and W. H. Pielemeier, J. Chem. Phys. **9**, 571 (1941).
[25] K. S. Pitzer, J. Chem. Phys. **5**, 473 (1937).
[26] E. B. Wilson and A. J. Wells, J. Chem. Phys. **9**, 319 (1941).
[27] K. S. Pitzer, J. Chem. Phys. **5**, 469 (1937).
[28] K. S. Pitzer and W. D. Gwinn, J. Chem. Phys. **9** 485 (1941).

give better agreement in the higher temperature region, but only at the expense of the present good agreement in the lower temperature region of the curve for measured C_v^0 values.

It should also be mentioned that the entropy of propylene calculated on the basis of the Wilson-Wells frequency assignment and a 2000-cal./mole potential barrier agrees with the measured entropy provided one assumes no entropy of mixing in the solid. On the other hand, if an entropy of mixing is assumed, the entropy calculated on Pitzer's basis agrees with the measured value. However, judging from the results of a study of cyclopentane by Aston and his co-workers,[29] an entropy of mixing cannot be expected in solid propylene.

ESTIMATED PRECISION OF MEASUREMENTS

If the wave-length frequency product λf is substituted for the velocity V in Eq. (7) one obtains

$$C_v=\frac{QR}{\{(\lambda f)^2M/RT-P\}}. \qquad (10)$$

The error of measurement present in C_v depends on the error of measurement in the three measured quantities λ, f, and T. One disadvantage of the sonic method of heat capacity measurements lies in the fact that a rather large propagation of errors is involved in the calculation of C_v. The quantity $(\lambda f)^2M/RT$ is approximately equal to the heat capacity ratio, C_p/C_v. Thus (since P is close to unity) the denominator of Eq. (10) will be from one-fourth to one-twelfth as large as $(\lambda f)^2M/RT$ itself, and consequently the relative error entering into Eq. (10) will be from four to twelve times as large as the relative error in $(\lambda f)^2M/RT$. For the propylene measurements, each of the quantities f^2, λ^2, and T were measured with a precision of 1 part in 2000, or better, and consequently the resulting C_v values, on the average, would be in error by about 0.6 percent because of errors in λ, f, and T. If additional precautions are taken in general technique, even greater precision than this should be possible.

Another quantity which may introduce error into the C_v determinations is uncertainty in the molecular weight M. As already stated, a specially purified sample of propylene was used for these measurements, and care was taken to retain its purity while measurements were being taken.

The 1937 international atomic weights (C $=12.010$ and H $=1.0078$) have been used. The ice-point has been taken as 273.16°K, and for the gas constant 8.3415×10^7 ergs/deg./mole, or 1.9869 cal./deg./mole has been used.

The author wishes to express his appreciation of the helpful criticism and guidance in this work given by Professor W. H. Pielemeier and Professor J. G. Aston, and of the stimulation and encouragement of his colleague, Dr. H. C. Hardy.

[29] J. G. Aston, J. Am. Chem. Soc. **63**, 2029 (1941).

Raman Spectra of Acetylenes

VI. 1-Butyne, 1-Pentyne, 1-Hexyne, 3-Hexyne, 4-Octyne and 1-Chloro-1-heptyne

FORREST F. CLEVELAND, *Department of Physics*, M. J. MURRAY AND H. J. TAUFEN, *Department of Chemistry*, *Illinois Institute of Technology, Chicago, Illinois*

(Received December 17, 1941)

Raman displacements, estimated intensities and depolarization factors have been obtained for $CH_3CH_2C\equiv CH$, $CH_3(CH_2)_2C\equiv CH$, $CH_3(CH_2)_3C\equiv CH$, $CH_3CH_2C\equiv CCH_2CH_3$, $CH_3(CH_2)_2C\equiv C(CH_2)_2CH_3$, and $CH_3(CH_2)_4C\equiv CCl$. The data obtained in the 2200 cm^{-1} region were [2068(1)P], 2118(10)0.5, 2158(3)0.5; [2064(0)], 2118(10)0.5; 2071(0), 2094(0), 2118(10)0.4; 2200(1)P, 2231(9)0.4, 2247(8)0.4, 2301(6)0.4; 2234(10)0.5, 2292(6)0.5; 2148(1)P, 2194(1)P, and 2243(10)0.4, respectively. Unusual features are the appearance of the second strong line at 2158 cm^{-1} in the spectrum of 1-butyne and the absence of the line near 2245 cm^{-1} in the spectrum of 4-octyne. Introduction of the Cl atom in the last compound radically modifies the spectrum in this region.

INTRODUCTION

DISUBSTITUTED acetylenes have more lines in the 2200-cm^{-1} region of the Raman spectrum than monosubstituted acetylenes. The present series of investigations[1] has been directed toward a better understanding of the reasons for this phenomenon. In particular, it was desired to observe the changes produced in this region when various substituents replaced one or both of the hydrogen atoms in the acetylene molecule.

In **I** and **II**, studies were made of a series of disubstituted acetylenes of the type $C_6H_5C\equiv CR$. It was found that the spectrum in the 2200 cm^{-1} region is quite sensitive to changes in the substituent *R*, the spectrum being dependent not only upon the atom or group immediately attached to the acetylenic carbon, but also upon the atom or group once or twice removed from it. In general, however, at least two strong lines with approximately equal depolarization factors were observed near 2215 and 2240 cm^{-1}.

Later, an infra-red investigation[2] of $C_6H_5C\equiv CCH_3$ was made in an attempt to test the Badger[3] hypothesis that Fermi resonance interaction was responsible for some of the additional lines in disubstituted acetylenes. While the frequency conditions for resonance did not seem to be very satisfactorily fulfilled, it was difficult to draw definite conclusions because of the uncertainty in regard to the effect of the anharmonicity upon the overtone frequencies.

In **III**, $C_6H_5C\equiv CI$ and eight substituted acetylenes not containing a phenyl group were studied. For the monosubstituted acetylenes, it was found that the substitution of a tertiary carbon atom caused a slight decrease in the 2118 cm^{-1} frequency and that in the case of $CH_3C(CH_3)(OH)C\equiv CH$ *two* strong lines, instead of the usual *one* for monosubstituted acetylenes, were observed at 2089(3) and 2112(10). Single lines were observed for two of the disubstituted acetylenes, but this is probably not significant since the line in one case was so broad as to suggest an unresolved doublet and in both cases the spectra were incomplete and a weak line could have gone unobserved.

In **IV**, it was shown that some of the weaker lines in the spectra of both monosubstituted and disubstituted acetylenes, having displacements smaller than that of the most intense line, may be due to isotopic molecules having C^{13} at one of the triple-bond positions, as originally suggested by Glockler and Renfrew for 2-butyne.[4]

An interesting case[5] is that of $CH_3(CH_2)_4C\equiv C(CH_2)_4CH_3$ in which the substitution of an oxygen atom for two hydrogen atoms to give

[1] I, J. Am. Chem. Soc. **60**, 2664 (1938); II, *ibid.* **61**, 3546 (1939); III, *ibid.* **62**, 3185 (1940); IV, J. Chem. Phys. **9**, 390 (1941); V, J. Am. Chem. Soc. **63**, 1718 (1941).

[2] M. J. Murray and Forrest F. Cleveland, J. Chem. Phys. **8**, 133 (1940).

[3] R. M. Badger, J. Chem. Phys. **5**, 178 (1937).

[4] G. Glockler and M. M. Renfrew, J. Chem. Phys. **6**, 408 (1938).

[5] M. J. Murray and Forrest F. Cleveland, J. Am. Chem. Soc. **63**, 1363 (1941).

$CH_3(CH_2)_4C{\equiv}CCO(CH_2)_3CH_3$ changed the spectrum from 2231(7), 2248(2), 2294(4) to a *single* line at 2212(7).

In **V**, several alkyl acetylenes were investigated. The two monosubstituted ones gave the strong line at 2118 cm^{-1} and also weak lines near 2064 and 2095 cm^{-1}, which may be due to the C^{13} isotopes. All of the disubstituted acetylenes gave a strong line near 2235, a slightly weaker one near 2295 and all except 9-octadecyne, for which the spectrum was incomplete, gave a weak line near 2250 cm^{-1}.

The present paper gives the results of an investigation of several of the lower members of the series of alkyl acetylenes. It was hoped that this investigation might provide some clue as to the origin of the line at 2250 cm^{-1}.

EXPERIMENTAL

The apparatus and experimental technique have been described[6] previously. The spectra were produced by use of Hg 4358A. Details in regard to the preparation and physical properties of the compounds are as follows:

1-Butyne, $CH_3CH_2C{\equiv}CH$, prepared from sodium acetylide and ethyl bromide according to the method of Vaughn, Hennion, Vogt, and Nieuwland,[7] b.p. 18–21°C.

1-Pentyne, $CH_3(CH_2)_2C{\equiv}CH$, prepared analogously, b.p. 41–43°.

1-Hexyne,[8] $CH_3(CH_2)_3C{\equiv}CH$, prepared analogously, b.p. 72°.

3-Hexyne, $CH_3CH_2C{\equiv}CCH_2CH_3$, prepared from sodium acetylide, sodamide and ethyl bromide, according to the method of Bried and Hennion,[9] b.p. 80.5–81.0°.

4-Octyne, $CH_3(CH_2)_2C{\equiv}C(CH_2)_2CH_3$, prepared analogously, b.p. 130.0–130.5°.

1-Chloro-1-heptyne, $CH_3(CH_2)_4C{\equiv}CCl$, from 1-heptyne to $C_5H_{11}C{\equiv}CNa$ by sodamide in liquid ammonia, thence, after removal of ammonia, to $C_5H_{11}C{\equiv}CCl$ by action of $CH_3C_6H_4SO_2Cl$ in ether, b.p. 58.0–58.4° at 35 mm pressure.

RESULTS

The results are given in Table I. The only compounds for which data seem to have been reported previously are 1-pentyne,[10] 1-hexyne[10, 11] and 3-hexyne.[12] Seven new lines were observed for 1-pentyne, and the 1446 line was resolved into the doublet 1432, 1454. The mean deviation of the present and former frequencies was 4 cm^{-1}, the maximum deviation being 12 cm^{-1} (for the 758 and 1044 lines). For 1-hexyne, eight new lines were found, the doublet 801, 814 appeared unresolved at 810 and the lines at 431 and 1024 were not found. The mean and maximum deviations were 2 cm^{-1} and 9 cm^{-1} (for the 2908 line), respectively. And finally, eleven new lines were observed for 3-hexyne, the 492 and 1447 lines were resolved into the doublets 484, 499 and 1439, 1460, the doublet 196, 211 appeared unresolved at 206 cm^{-1} and the 321 and 1144 lines were not found. The mean and maximum deviations were 1 cm^{-1} and 3 cm^{-1}, respectively. Depolarization factors do not seem to have been reported heretofore for any of the present compounds.

DISCUSSION OF RESULTS

Frequencies Near 2200 cm^{-1}

Monosubstituted Acetylenes

The Raman data obtained in this laboratory for a number of monosubstituted acetylenes are collected in Table II; 1-propyne is also included in the table for completeness. The weak lines near 2066 and 2095 may be ascribed to the triple-bond frequencies of the two possible C^{13} isotopes (see **IV**). The strong line at 2124 cm^{-1} for 1-propyne drops to 2118 for 1-butyne and retains this value for higher members of the series, as well as for many other monoalkylacetylenes. For 1-butyne, an additional line of medium intensity was observed at 2158 cm^{-1}. This line may be due to Fermi resonance interaction between the triple bond fundamental and

[6] J. Chem. Phys. **7**, 396 (1939); *ibid.* **8**, 153 (1940); *ibid.* **10**, 18 (1942).
[7] T. H. Vaughn, G. F. Hennion, R. R. Vogt, and J. A. Nieuwland, J. Org. Chem. **2**, 1 (1937).
[8] Synthesized by Mr. R. E. Dineen and spectrograms measured by Mr. Robert D. Sieg.
[9] E. A. Bried and G. F. Hennion, J. Am. Chem. Soc. **59**, 1310 (1937).
[10] R. Courtel, Diplôme d'études supérieures, Paris, 1932.
[11] M. Bourguel and P. Daure, Bull. Soc. Chim. **47**, 1349 (1930).
[12] H. Van Risseghem, Bull. Soc. Chim. Belg. **47**, 271 (1938).

TABLE I. Raman spectra of some acetylenes.

1-Butyne			1-Pentyne			1-Hexyne			3-Hexyne			4-Octyne			1-Chloro-1-Heptyne		
$\Delta\nu$	I	ρ	$\Delta\nu$	I	ρ	$\Delta\nu$	I	ρ	$\Delta\nu$	I	ρ	$\Delta\nu$	I	ρ	$\Delta\nu$	I	ρ
			[*120*	3	0.9]												
			±174	5b	0.8							[165	2b]				
±206	8vb	0.7				±204	4	0.8	±206	6vb	0.8				±262	3b	0.7
						272	1										
290	1	P													±335	2	
±348	5b	0.7	±341	6b	0.9	±339	6	0.8				342	1				
									±364	3vb	0.7	±371	5	0.9	±357	7	0.7
						±383	4	0.4									
												468	2b	0.7	427	2	0.8
									484	1							
509	4	0.5	498	2	0.4	504	2	P	499	3	0.7	[509	0]		492	2b	0.8
			532	2	0.7				*532*	2		534	0				
						552	1					551	1				
563	3	0.5															
												578	1				
															602	1	P
642	3vb	0.7	632	3vb	0.9	632	3vb	0.8									
									681	2		674	2	0.9			
									695	2							
			758	1	0.5												
784	½								782	3	P				777	0	
												808	3	0.4			
840	7	0.2	837	5	0.2	810	5	0.6							834	4	0.6
												855	4	0.5			
			871	3	0.4	874	1	P							872	1	
						897	1					891	5	0.5	890	1	0.8
			[*924*		0.9]	932	2b	P	918	2					913	1	0.9
															961	1b	0.8
						[979	0]		983	7	0.3						
															995	1	[0.9]
1005	3	0.6															
1023	1											1020	1	0.9	1023	1	[0.9]
			1044	2	0.7							1037	2				
1068	6	0.3				1055	5	0.7	1064	8	0.3	1069	1	0.9	1060	2	0.7
			1094	3	0.6							1095	4	0.5	1089	2	0.9
						1106	5	0.7							1112	3	0.6
						[*1208*	0]		*1207*	½							
			1228	1	0.9	*1238*	½					1227	2	0.6	1220	1	P
1252	1b	0.6	*1261*	2	0.7				1259	2	0.9	1260	3	0.6			
												1274	1		1270	0	
			1300	1	0.9	1298	3	0.7				1291	1		1303	3	0.7
1314	4	0.6							1319	7	0.6						
			1327	2	0.9	1328	3	0.7				1327	5	0.6	1330	3	0.7
						[*1356*	0]					1350	2	P			
1375	1								1376	2	P						
1438	4b	0.8	1432	4	0.9	1439	5	0.9	1439	5	0.7	1434	5	0.8	1436	5	0.7
1459	3b	0.8	1454	5		1456	3		1460	4	0.8	1456	4b	0.8	1457	3	0.7
[2068	1	P]	[*2064*	0]		*2071*	0										
						2094	0										
2118	10	0.5	2118	10	0.5	2118	10	0.4									
2158	3	0.5													2148	1	P
									2200	1	P				2194	1	P
									2231	9	0.4	2234	10	0.5			
									2247	8	0.4				2243	10	0.4
									2301	6	0.4	2292	6	0.5			
						2714	½										
2734	1	P	*2740*	3	P	*2737*	1		*2729*	2	P	2736	2	P	2725	1	P
2851	3	0.4	2838	4	0.5	2839	2		*2850*	5	0.2	2841	5	0.4	2856	6	0.3
2885	5b	0.4	2871	7	0.2	2869	8	0.5	*2883*	4	0.3	2871	8	0.2	2874	6	
2919	7	0.2	2908	8	0.5	2908	9	0.5	*2909*	10b	0.3	2905	9	0.5	2908	8	0.3
2941	8	0.2	2939	8	0.5	2933	9	0.4	*2939*	10	0.1	2936	9	0.4	2936	8	0.2
2986	5	0.8	2972	5	0.8	2965	6	0.9	*2978*	7	0.7	2971	6	0.9	2965	5	0.9
3305	2	0.6	3304	4	0.7	3303	2	P									

$\Delta\nu$ = Raman displacement in cm^{-1}, I = estimated intensity, ρ = depolarization factor, ± indicates observation both as Stokes and anti-Stokes lines, brackets enclose data in regard to which there is some question, b = broad, vb = very broad, P means that ρ was less than 6/7 but that it was not possible to make a quantitative measurement, the brace joins lines that were unresolved on the polarization spectrogram, and bold type indicates previously observed frequencies.

the first overtone of the strong, polarized Raman line observed at 1068 cm^{-1}. However, several combinations of the observed Raman frequencies fall in this region and it may be that one of these combination frequencies is involved in the resonance interaction that accounts for the additional line. Another possibility is that an overtone of a vibration (or a combination of two vibrations) that is active in infra-red absorption but weak or absent in the Raman spectrum may be the one involved in the resonance interaction. It is hoped that the infra-red spectrum may soon be obtained in this laboratory and that perhaps this additional information may make possible a more definite explanation of the occurrence of the 2158 line.

Disubstituted Acetylenes

The Raman data for the 2200 cm^{-1} region of the spectra of several dialkylacetylenes are collected in Table III. The weak lines at 2201 and 2280 cm^{-1} in the spectrum of $CH_3C\equiv CCH_3$ have been attributed[4] to the isotopic molecule $CH_3C^{13}\equiv C^{12}CH_3$ and it seems possible that the weak line near 2198 cm^{-1} in the spectra of the other dialkylacetylenes may have a similar origin (see **IV**). It seems probable that the two strong lines near 2233 and 2300 result from Fermi resonance interaction between the triple-bond fundamental and the first overtone of the antisymmetrical, infra-red active, vibration of the $C-C\equiv C-C$ group, as for the well-known case of 2-butyne.[13] If this is true, the infra-red frequency should remain practically constant at 1126 cm^{-1}, the value for 2-butyne. Experiments to test this point are a part of the future program of this laboratory.

In addition to the above frequencies, a line appears near 2250 cm^{-1} in the spectra of all of the dialkylacetylenes measured in this laboratory, with the exception of 9-octadecyne and 4-octyne. For the former, the spectrum was incomplete and the line may actually exist, but for the latter the spectrograms were excellent, with no trace of the line, either on long or short exposures. It is remarkable that the line should be absent for 4-octyne in view of its great intensity in the next lower member of the series, 3-hexyne. Several combinations of the observed Raman frequencies fall in this region, but it does not seem possible upon the basis of these combination frequencies to account simultaneously for the great intensity of the 2250 line in 3-hexyne, its appearance with smaller intensity in the spectra of other dialkylacetylenes and its strange absence in 4-octyne.

The spectrum of 1-chloro-1-heptyne was obtained to see how the spectrum in the 2200 cm^{-1} region would be affected by replacing the hydrocarbon group by a single atom of a different kind. As Table I shows, the 2233, 2300 doublet of the alkylacetylenes is replaced by a single strong line at 2243 cm^{-1}. This would be understandable if it were assumed that the antisymmetrical, infra-red frequency near 1100 cm^{-1} were shifted to a value too low to produce a strong resonance interaction with the triple-bond fundamental. The two weak lines observed at 2148 and 2194 cm^{-1} may arise from weak resonance interactions of the first overtone of the lowered 1100 frequency and one of the combination frequencies that fall in this region with the triple-bond fundamental.

TABLE II. Raman spectra of monoalkylacetylenes, $R(CH_2)_nC\equiv CH$, near 2200 cm^{-1}.

R	n	$\Delta\nu(I)\rho$				Reference
CH_3	0			2124(10)		a
CH_3	1	2068(1)P		2118(10)0.5	2158(3)0.5	b
CH_3	2	2064(0)		2118(10)0.5		b
CH_3	3	2071(0)	2094(0)	2118(10)0.4		b
CH_3	4	2064(0)	2097(0)	2118(10)0.4		c
OCH_3	2	2064(0)	2094(0)	2118(10)0.4[d]		c

[a] G. Glockler and H. M. Davis, J. Chem. Phys. **2**, 881 (1934); Bryce L. Crawford, Jr., *ibid.* **8**, 526 (1940).
[b] This investigation.
[c] This laboratory, see **V**.
[d] Careful remeasurement of the depolarization factor for this line indicates that the previously reported value of 0.2 should be corrected to 0.4.

[13] Cf. Bryce L. Crawford, Jr., J. Chem. Phys. **7**, 555 (1939).

TABLE III. Raman spectra of dialkylacetylenes, $CH_3(CH_2)_nC\equiv C(CH_2)_mCH_3$, near 2200 cm^{-1}.

n	m	$\Delta\nu(I)\rho$				Reference
0	0	2201(1)	2235(7)P	2280(1)	2313(6)P	a
0	1		2238(10)		2304(4)	b
0	2		2238(10)		2304(4)	b
0	3		2235(8)		2303(4)	b
0	4	2198(0)	2233(10)0.4	2256(1)	2305(8)0.4	c
0	5		2233(6)		2303(4)	b
1	1	2200(1)P	2231(9)0.4	2247(8)0.4	2301(6)0.4	d
1	3	2199(0)	2235(8)0.4	2249(1)	2296(6)0.4	c
1	4		2232(8)		2293(4)	b
1	5		2232(8)		2294(4)	b
2	2		2234(10)0.5	——	2292(6)0.5	d
2	4		2234(8)		2293(4)	b
2	5		2233(8)		2292(4)	b
3	3	2195(0)	2233(8)0.4	2245(2)0.4	2296(5)0.4	c
3	4		2231(8)		2293(4)	b
3	5		2233(8)		2294(4)	b
4	4		2231(7)0.4	2248(2)	2294(4)0.4	e
5	5		2233(7)0.4	2252(2)0.4	2294(5)0.4	c
7	7		2231(7)		2290(4)	c

[a] Mean values, see Crawford's summary of data, reference 14.
[b] Blanche Gredy, Thèses, Paris, 1935.
[c] This laboratory, see **V**.
[d] This investigation.
[e] This laboratory, see **III**.

Other Frequencies

The strong, very broad line near 206 cm^{-1} in the spectra of 1-butyne, 1-hexyne, and 3-hexyne unexpectedly drops to 170 cm^{-1} in the spectra of the propylacetylenes 1-pentyne and 4-octyne.

The strong lines near 340 and 630 cm^{-1} for the monosubstituted acetylenes and near 365 for the disubstituted acetylenes were observed also for the alkylacetylenes in **V**. Following Crawford,[13] the frequency near 630 may be identified with the bending of the $C\equiv C-H$ angle and the ones near 350 may be associated with the $C\equiv C-CH_3$ angle.

All the present compounds, as well as four of the seven alkylacetylenes in **V**, have a line near 500 cm^{-1}. The present compounds also have, without exception, a polarized line near 800 and lines near 1065 and 1250 cm^{-1}. Lines near 1300 and 1330 were found for the four compounds having a fairly long chain (and for five of the compounds in **V**), but not for the two containing only ethyl groups; these two, however, have lines at 1315 and 1375 cm^{-1}. The doublet observed at 1440, 1457 (mean values) for the seven alkylacetylenes in **V** appears here at 1436, 1457.

MARCH, 1942 JOURNAL OF CHEMICAL PHYSICS VOLUME 10

The Raman Spectra of the Sugars in the Solid State and in Solution

I. The Raman Spectra of α- and β-*d*-Glucose*

FRANK H. SPEDDING AND ROBERT F. STAMM
Plant Chemistry Subsection, Agricultural Experiment Station† and Department of Chemistry, Iowa State College, Ames, Iowa

(Received December 11, 1941)

This paper presents data on the Raman spectra of anhydrous crystalline α- and β-*d*-glucose and of equilibrium aqueous *d*-glucose solutions containing 5, 15, and 50 moles of water per mole of glucose. Ultraviolet excitation (Hg λ2537A) was employed. A technique for photographing Raman spectra of crystalline organic powders and solutions with very poor scattering power is described. It consisted essentially of the use of complementary filters of aqueous succinic acid (saturated, 4 mm thick) and a mercury vapor absorption cell (10 cm long, 150°C). Thirty-six lines are reported for α-*d*-glucose, 32 for the β, and numerous new bands including measurements of maxima and shoulders are given for equilibrium solutions. Only the obvious experimental differences are discussed as the detailed discussion will be given in a later paper of this series.

INTRODUCTION

THE carbohydrates play such an important role in agricultural chemistry that additional knowledge about their structures and chemical and physical properties is greatly to be desired. Because of the complexity of these compounds, accurate experimental work is difficult and there is a great need for the development of new physical methods to help the investigators in this field. The Iowa Agricultural Experiment Station, therefore, in collaboration with the Chemistry Department has started a program to study the Raman spectra of the sugars and their derivatives. It is hoped that the method and technique of the Raman effect can be developed so as to be a useful tool in this field. If the Raman spectra of the various sugars could be photographed readily in the solid state and in solution, then from the differences in their vibrational frequencies it should be possible to identify the sugars by their spectra and even to determine quantitatively the amount of one sugar in the presence of another providing the mixture was not too complicated. Chemically this can be done only with great difficulty. In addition to this if the frequencies of a given sugar in the solid state differ from those in solution, some light might be thrown on the sugar-sugar and sugar-water association. Also, since the frequencies may be compared with those of mole-

* From the dissertation to be submitted by Robert F. Stamm to the Iowa State College in partial fulfillment of the requirements for the degree of Doctor of Philosophy.
† Journal Paper No. J.954, Project 696.

cules thought to be similar and having better known geometrical structures, an insight into the structures of the sugars might thus be obtained. Finally, a complete set of vibrational frequencies would permit a dynamical analysis to be made with the resultant proof of geometrical structure. This last objective presents well-nigh insuperable difficulties if carried out rigorously by the usual methods. However, as the theory develops and the newer calculating machines‡ become available, even this might be accomplished if the vibratory frequencies are available.

In this, the initial paper of a series, we are reporting the Raman spectra of α- and β-*d*-glucose in the solid state and that of equilibrium *d*-glucose in solution. This aldo-hexose is one of the most important since it is the building block of both starch and cellulose.

Several investigators of Raman spectra have worked with the sugars, including *d*-glucose, in the past with partial success. Whiting and Martin[1] examined a dextrose solution of 500 g per liter. They found no Raman lines, only an undiminished continuum. Kutzner[2] obtained three lines of very low intensity accompanied by a heavy continuum after 30 hours' exposure. Wiemann[3] used charcoal to decolorize a 30 percent dextrose solution which he then filtered through sintered glass and reported that very little continuum was present in his pictures. He found eleven bands in solution. A. L. Sundara Rao[4] reported twelve lines for *d*-glucose solution, two of them broad. Only the last investigator reported any lines in the C−H and O−H regions and he stated that the spectra were so faint that it was difficult to distinguish them from the background.

Since the glucose frequencies can also be observed in infra-red absorption, it should be mentioned that Coblentz[5] studied molten dextrose and obtained a band from 3–4μ and a maximum at 4.8μ. Rogers and Williams[6] used saturated solutions 0.002 mm thick and investigated the region 2–12μ. They reported seven bands but could not resolve details in the C−H and O−H regions. Barr and Chrisman[7] evaporated saturated solutions on cover glasses and used the resulting syrups. Two bands were found by them for each of a series of sugars including *d*-glucose.

The phenomenon of muta-rotation leads to the conclusion that in aqueous glucose solutions both the α- and β-forms of the pyranose ring are present in equilibrium with one another and perhaps in equilibrium with other forms. Therefore any spectrum of the solution will be composed of a superposition of the spectra of all the various forms present and many of the bands observed will in reality be envelopes of several lines or bands from these forms. Since all of the above work (that of Coblentz excepted) was done with equilibrium solutions, the values of the vibrational frequencies obtained by them should be compared with our solution values in Table I.

The α- and β-forms of *d*-glucose are geometrically different and should possess different vibrational frequencies. It is therefore desirable to study the spectra of the pure forms alone. This can be done with the sugars in the solid state.

EXPERIMENTAL

From the work of Kwiencinski and Marchlewski[8] and especially from that of V. Henri and Schou[9] it was decided that pure *d*-glucose does not absorb light of wave-lengths longer than 2300A and that the 2537 mercury line could therefore be used as a primary exciter of the Raman lines. We employed one of the low pressure argon-mercury arcs.[10] Unfortunately the direct light from this arc decomposes all sugars so that all light below 2300A has to be removed by a filter.

‡ Those used for evaluating secular determinants.

[1] Whiting and Martin, Trans. Roy. Soc. Can. III [3] **25**, 87–98 (1931). (Visible Hg excitation, quinine sulphate filter.)

[2] Kutzner, Naturwiss. **20**, 331–332 (1932). (Supersaturated solution at 20°C, quartz Hg arc, visible excitation.)

[3] Wiemann, Comptes rendus **203**, 789–791 (1936). (Visible Hg excitation.)

[4] A. L. Sundara Rao, Indian J. Phys. **14**, 207 (1940). (Visible Hg excitation.)

[5] W. Coblentz, Carnegie Inst. of Wash. Pub. **65** (1906).

[6] Rogers and Williams, J. Am. Chem. Soc. **60**, 2619–2621 (1938).

[7] Barr and Chrisman, J. Chem. Phys. **8**, 51–55 (1940).

[8] Kwiencinski and Marchlewski, Bull. Soc. Chim. **43**, 725–743 (1928).

[9] V. Henri and Schou, Zeits. physiol. Chem. **174**, 295 (1928).

[10] The Hanovia Chemical and Manufacturing Company, Newark, New Jersey (Helicoidal type, 0.1 amp. at 4400 v).

TABLE I.

Anhydrous α-d-glucose	Int.	Anhydrous β-d-glucose	Int.	5 moles H_2O: mole glucose	Int.	15 moles H_2O: mole glucose	Int.	50 moles H_2O: mole glucose	Int.	Previous investigators solutions only
142	1	137	1	96		121		90		
168	1	163[1]	1	i. 171	1	187	1	i. 172	1	
224	1			247		252		255		
				288				255		
				i. 302	0			i. 290	0	
				316				325		
				322		327		336		
				i. 345	1	m. 349	1	i. 349	1	
				368		359		363		
363	0					371				
				386		m. 385	1	389		
395	4			sh. 410		m. 407	6	m. 404	3	
405	4	404	3	m. 423	7[2]	m. 423	8[2]	m. 421	6[2]	423(R)
		425	0	m. 445	6	m. 448	6	m. 447	4	435 ±25(W), 454(K)
441[1]	1			467		469		m.? 464	3	
		462	0					471		
				483		483		486		
				sh. 502		m. 498	5	m. 497	4	
		523	3	m. 518	6	m. 518	8	m. 520	5	519 ±11(W), 513(K)
				sh. 540	1	m. 542	6	m. 541	4	549[3](R)
542	8			m. 550	0					
		567	0	m. 562	0	m. 562	0	m. 559	0	
								m. 573	2	
				m. 584	0	m. 588	0	m. 586	0	
580	0			589		597		609		
				628		628				
				i. 640	0	m. 636	2			624[1](R)
				652		658				
						? 694	0	687		
				702		705		i. 707	0	
				m. 715	2	m. 720	0			
				730		739		727		
				760		744		750		
				m. 775	2	m. 768	1	i. 773	2	
774	2			794		795		796		
				798		795				
				m. 804	1	m. 814	1			
				812		829				
		825	0	829		829		835		
				m. 845	4			m. 850	3	
842	8			m. 858	4	m. 856	3			856(R), 853 ±10(W)
		870	0	sh. 870				m. 868	3	
				872		878		875		
				879		878		893		
		901	3	sh. 894		m. 899	5	m. 905	4	
887	0	914	0	m. 911	5	m. 914	5	m. 916	4	919(R), 911 ±14(W)
913	6	941	0	sh. 930	3	sh. 937		937		
				951		951				
				970				982		
				m. 986	2	999		m. 998	3	1000(RW)
				1016		m. 1016	6			1020 ±10(W)
				m.	5					
1020	1	1025	1	1029						
				sh. 1038	6	m. 1033	7			
? 1038[1]	1			m. 1066	8	m. 1063	10	m. 1069	7	1064[7] br. (R), 1067 ±12(W)
1057	5	1051	3	sh. 1080	7	sh. 1076		sh. 1082		
1072	6			1085		1089		1089		
				1091		1089		1095		
								sh. 1101		1100(RW)
1109	5d.									
		1118	4	m. 1124	11	m. 1126	13	m. 1124	11	
1122	6	1130	4							
1149	4	1151	0	sh. 1152	6	sh. 1155		sh. 1158		1159[10] br. (R), 1145 ±9(W),
				1179		1176		1184		1140(K)
				1187		1193				
1203	1	1209	0	m. 1200	2	i. 1206	2			1200(W)
						1219				
				sh. 1230	3	1219		1222		
				sh. 1252		m. 1233	4	m. 1233	3	
? 1227[1]	1			m. 1265	5	m. 1263		m. 1247	4	
1273	2	1268	2	sh. 1284	1		6	m. 1269	5	1270(R), 1262 ±8(W)
				1286		1292		1285		

This was done by circulating a saturated (30°C) aqueous solution of succinic acid continuously through a fused-quartz filter jacket interposed between the arc and the Raman tube. The thickness of the filter solution was 4 mm and it was circulated by means of a midget centrifugal pump.[11] A number of other solutions were tried but proved unsatisfactory; e.g. sodium succinate tended to give off gas which permitted the short ultraviolet light to get through where the bubbles

[11] Obtainable from the Eastern Manufacturing Company, New Haven, Connecticut.

TABLE I—*Continued.*

Anhydrous α-*d*-glucose	Int.	Anhydrous β-*d*-glucose	Int.	5 moles H_2O: mole glucose	Int.	15 moles H_2O: mole glucose	Int.	50 moles H_2O: mole glucose	Int.	Previous investigators solutions only
? 1302	0	1312	0	1295		1292		1302		
		1336	0	m. 1331	5	m. 1337	8	m. 1333	7	
1345	6	1350								
		1363	2							
1374	1	1377		m. 1370	10	m. 1371	11	m. 1373	8	1370(R), 1373±19(W),
br.d. 1417	1	br. 1407	1	sh. 1411	5	m. 1413	6	1417		1370(RW)
				m. 1430	3	1427				
				1436						
				1444		1444		1449		
1461	5	1452	2	m. 1462	7	m. 1460	8	m. 1465	5	1463(R), 1464±7(W)
				1490		1496		1485		
		1507	0							
				1605		1584		1588		1590(RW)
		$\nu\delta(H_2O)$		i. 1646	0	i. 1642	3	1646	5	
				1688		1701		1706		1670(RW)
				2057		2065		2053		
		(H_2O)		i. 2168	3	i. 2140	2	i. 2172	3	2080(RW)
				2280		2214		2292		
				2447						
				2528	0					
				2549						
				2556						
								2596		
				br.m. 2625	4			*		
2640								i. 2641	3	
						2669				
								2686		
i. 2700	1					i. 2710	2	2686		
				br. 2706						
2761				i.flat 2744	7	2750		i. 2737	6	
2833				m. 2781				2788		
i.d. 2856[1]	1							2788		
2879				sh. 2801		2805				2805; br. (R)
2879	15	d. 2876[1]	4					br. 2876		
2893	20	2895	20	br.m. 2896	20	m. 2902	20	m. 2890	20	
2916	8	2908	20					2904		
		2929	4							
2946	19	2947	13	br.m. 2945	16	m. 2943	17	m. 2953	16	
2961	12	2977	13	3022		3015		2991		
				3047		3015		3011		3030(RW)
				3189		c.		3168		
				3231	20	br. 3237	20	br.		3260 br. (R)
				3276		m.		i. 3271	30	
3396	4			3349		c.		m. 3374		
				br.m. 3439	30	br. 3434	24			
		3503		3522		m.				
		3556	1			3619				
				3714				3738		

[1] Observed on only one plate.

[2] From the relative intensities of Hg λ2563.9 and 2578.4A, we conclude that this maximum is not the mercury line 2563.9A but is a Raman line. br. broad, c. center, d. diffuse, i. center interpolated, m. maximum, sh. shoulder, ? doubtful. (K) Kutzner, reference 2, (R) Rao, reference 4 (subscripts are his intensities), (RW) Rogers and Williams, reference 6, (W) Wiemann, reference 3.

formed and the sugar was then decomposed because the bubbles did not always leave the cell immediately. The succinic acid[12] proved very satisfactory. The ultraviolet arc emits the 1850A line of mercury with considerable intensity. This in turn generates ozone in the air which tends to cut down the intensity of ultraviolet light reaching the spectrograph. The difficulty was overcome by having a strong suction just above the arc so that the ozone was removed as soon as it was formed.

The sugar crystals were contained in a fused-quartz tube of 6 mm inside diameter with a fused-quartz window sealed on the end. The length of the sample was about 5 mm. Longer samples were not needed since very little light penetrated to the window from distances greater than 5 mm. In order to prevent light which had not penetrated the crystals from reaching the spectrograph a brass collimator containing two diaphragms of 4-mm aperture placed 3 inches apart was affixed to the tube with Duco cement. The interior of the collimator was painted a flat black. To gain better light transmission some of the very fine crystalline powders were moistened with absolute methyl alcohol. Only one line of the methyl alcohol appeared on any of the plates ($\Delta\nu$ 2836 cm^{-1}). With the dispersion used, no change in the frequency of the sugar vibrations could be detected when this procedure was used and the exposure time was cut frequently by a third.

[12] The quantitative absorption data can be found in the paper by Ley and Arends, Zeits. f. physik. Chemie **B17**, 177 (1932).

The sugar solutions were filtered through sintered glass and placed in a fused quartz Wood's tube with a flat, polished window.[13] This tube had a diameter of 15 mm and a possible active length of 5 inches. A half-inch length of the front of the tube and the horn were painted a flat black thus leaving a 3-inch effective length for irradiation. The solution tube had a collimating tube also and was used in conjunction with the filter jacket mentioned above. The mercury arc was surrounded with a polished sheet aluminum reflector, and the entire assembly was located in a large box. The collimator tube projected through the box, thus eliminating the possibility of light from the arc getting into the spectrograph. In the case of powders there can be no (or at most only a very short) dead optical space in the front end of the sample, for unless the powder near the window is illuminated, the secondary radiation cannot get through to be photographed. Thus with the powders considerable primary light (except 2537 which was especially removed) got into the spectrograph due to multiple reflections from the crystal faces, and the continuum on each side of 2537 was strong as were the rest of the mercy lines. Since this arc yields a particularly strong resonance line (the makers claim it to be nearly 80 percent monochromatic 2537), on long exposures, we found that the usual practice of having mercury vapor in the spectrograph to absorb the 2537 line was not efficient enough and we therefore employed a mercury vapor absorption cell. This cell was electrically heated, had an absorbing column 10 cm long, and when heated to *ca.* 150°C with a drop of mercury in it, completely obliterated the 2537 line.

The spectrograph employed was a Bausch and Lomb medium quartz type. In the region used the linear dispersion ran from around $7\frac{1}{2}$–9A/mm. The room housing the spectrograph was thermostated to within 1°C.

The sugars used were anhydrous α-*d*-glucose,[14] $[\alpha]_D^{0.2°C} = 110.4$ initial rotation (Lit. 111.5); $[\alpha]_D^{30°C} = 52.2$ final rotation (Lit. 52.7): α-*d*-glucose monohydrate,[15] $[\alpha]_D^{0.2°C} = 100.8$ initial rotation (Lit. 101.4); $[\alpha]_D^{30°C} = 47.5$ final rotation (Lit. 47.9): anhydrous β-*d*-glucose (two samples), one (from The Pfanstiehl Chemical Company), $[\alpha]_D^{0.2°C} = 18.5$ initial rotation (Lit. 18.4); $[\alpha]_D^{30°C} = 52.5$ final rotation: another (prepared according to Hudson and Dale[16]), $[\alpha]_D^{0.2°C} = 18.5$ initial rotation; $[\alpha]_D^{25°C} = 51.8$ final rotation. The literature specific rotation values given were taken from the paper by Isbell and Pigman.[17] Unfortunately their figures do not agree exactly with those of other investigators and the discrepancies are of the same magnitude as those between our values and those of Isbell and Pigman. Therefore, all we can say about the purity of our α- and β-sugars is that any impurities or other forms present must be there in such small amounts that their Raman spectra would not be observed. The solution pictures were made with *d*-glucose purified by the method of Hudson and Dale[16] using "Cerelose" as starting material.[18] A solution of "Cerelose" is usable but is slightly yellow originally and is a very bright yellow after a 24-hr. exposure. Also the impurities which can be removed by clarification and recrystallization increase the exposure time and give rise to fluorescence thus tending to hide the fainter Raman lines.

It was found difficult to measure the lines under our comparator since due to its magnification and to the low contrast of the fast plates used, the lines tended to wash out. Therefore the spectrograms were enlarged about sevenfold on high contrast paper and the wave-lengths of the Raman lines found by the Hartmann formula. Such was not the case, however, for the solution bands since they were frequently envelopes of a number of lines often diffuse and ill defined. It was found better to microphotometer these plates with a tenfold enlargement and to measure the band edges, shoulders, and maxima on the curves and to determine their wave-lengths by means of the Hartmann formula. Checks of the solution measurements were made on enlarge-

[13] This and the filter jacket were obtained from The American Instrument Company.

[14] "Cerelose" from the Corn Products Company, New York.

[15] Prepared according to Hudson and Yanovsky, J. Am. Chem. Soc. **39**, 1013 (1917).

[16] Hudson and Dale, J. Am. Chem. Soc. **39**, 320 (1917).

[17] Isbell and Pigman, J. Research Nat. Bur. Stand. **18**, 158 (1937).

[18] In the clarification both "Norit" and SO_2 were used prior to the concentration and subsequent crystallization.

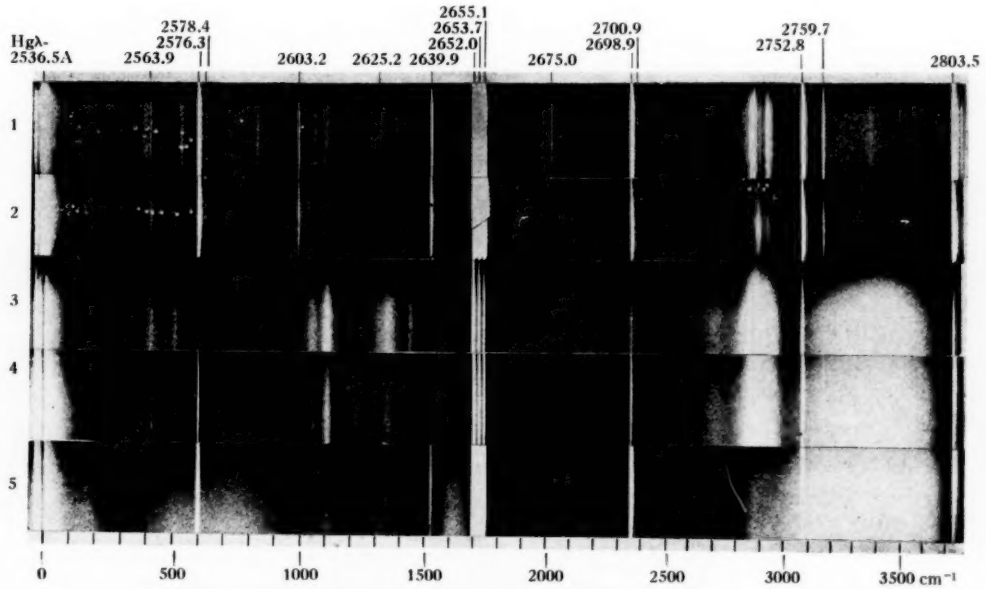

FIG. 1. Enlargements representative of the Raman spectra obtained by Hg λ2537A excitation. 1. Anhydrous *α-d*-glucose. 2. Anhydrous *β-d*-glucose. 3. 5 moles H_2O/mole glucose. 4. 15 moles H_2O/mole glucose. 5. *ca.* 520 moles H_2O/mole glucose (0.1 molar). The two bands in 1 and the higher of these two bands in 2 lying to the low side of Hg 2803.5A belong to a band system in the arc which encroaches slightly on the O-H region.

ments to be sure that no false information (due to scratches or flaws on the plates) would be conveyed by the curves. Too much stress must not be put on these band edges since their position varied slightly with the time of exposure. The low frequency "crystal" lines on the crystal plates were measured on the comparator after first pricking the lines with a fine needle.[19] In general the measurements are judged to be accurate to within ± 2 cm^{-1}. The intensities are qualitative only and are based on a scale of 0 to 20 with 2893, 2895–2908, and the 2900-cm^{-1} band of the *α-*, *β-*, and solution plates respectively being given an arbitrary rating of 20. Plates were made of the direct arc in order to be sure which lines originated in the arc and which in the sugar.

Below is given a resumé of plates measured. After the number of the plate, the words "dry" or "moistened" indicate whether the powder was photographed dry or moistened with absolute methyl alcohol. Next is given the slit width on the spectrograph and finally the number of hours which the plate[20] was exposed.

α-d-glucose anhydrous (all I-O plates): (1) dry, 0.025 mm, 35 hr. (2) dry, 0.02, 25 (3) moistened, 0.02, 15 (4) moistened, 0.02, 25.

β-d-glucose anhydrous (all I–O plates): (1) moistened, 0.02, 24 (2) dry, 0.02, 60 (3) dry, 0.04, 72 (4) moistened, 0.03, 40 (5) dry, 0.03, 42 (6) dry, 0.03, 72.

Saturated equilibrium *d*-glucose (*ca.* 5 moles H_2O/mole glucose): (1) I–O, 0.025, 25 (2) 103–0, 0.04, 75 (lines also confirmed on two other plates not measured).

Dilute equilibrium *d*-glucose (*ca.* 15 moles H_2O/mole glucose): (1) 103–O, 0.03, 84.

Dilute equilibrium *d*-glucose (*ca.* 50 moles H_2O/mole glucose): (1) 103–O, 0.03, 47 (lines confirmed on other plates not measured).

The results are summarized in Table I. The strong lines were observed and measured on all plates mentioned. In the first three columns the weaker lines were observed and measured on at least two plates unless marked by a superscript 1 in the table.

[19] Some of these low $\Delta\nu$ lines seen in the reproductions may arise in the arc. They are $\Delta\nu$ 47, 79, 111, 191, and 380 cm^{-1}. These arc lines are sharp but faint and probably too many crystal frequencies were rejected by being assigned to these weak lines in the source. We have leaned over backwards in this respect.

[20] All Eastman plates.

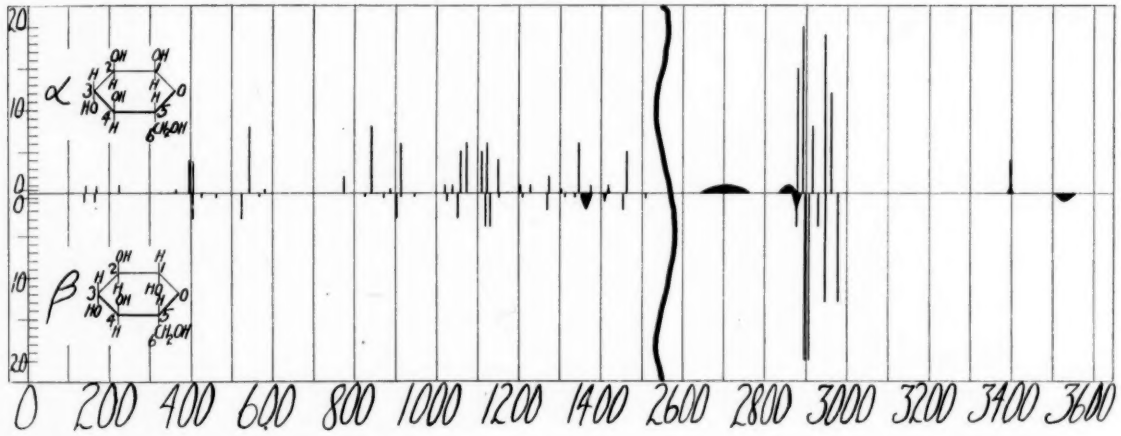

FIG. 2. Comparison of the Raman frequencies (in cm^{-1}) of anhydrous α- and β-*d*-glucose. Intensity estimates plotted vertically.

DISCUSSION OF RESULTS

In the crystals there is only a fair one-to-one correspondence among the vibrational frequencies of α- and β-*d*-glucose below 1500 cm^{-1}. One notable discrepancy is the absence of a strong frequency in the β-*d*-glucose near the rather intense 842-cm^{-1} line of the α-form. While it is a fact that a strong frequency exists in this region for a whole series of six membered heterocyclic ring compounds and corresponds to the breathing frequency, we do not wish to make any conjecture about the absence of a strong frequency of the β-form in this region until more intense spectrograms have been taken along with accurate intensity measurements and polarization characteristics of the lines. We hope to carry out these experiments if we are successful in growing large single crystals free from fluorescent impurities and flaws. The most striking difference between the two crystalline forms is exhibited in the 2900-cm^{-1} region where the form of sugar may be identified by a glance at the spectra. The O—H frequency region is nearly bare for both forms with only one line in the α and one band in the β. On the best plates, which we have reproduced in Fig. 1, there is some evidence in the α for another frequency of slightly smaller value than the O—H frequency mentioned. Rough preliminary measurements on the α-monohydrate seem to show no marked differences from the anhydrous α. This seems astounding and we are investigating the spectra further. We do not feel that speculation as to the identity of the various frequencies or as to their appearance or non-appearance would be very profitable at this time. We are, therefore, reserving any such

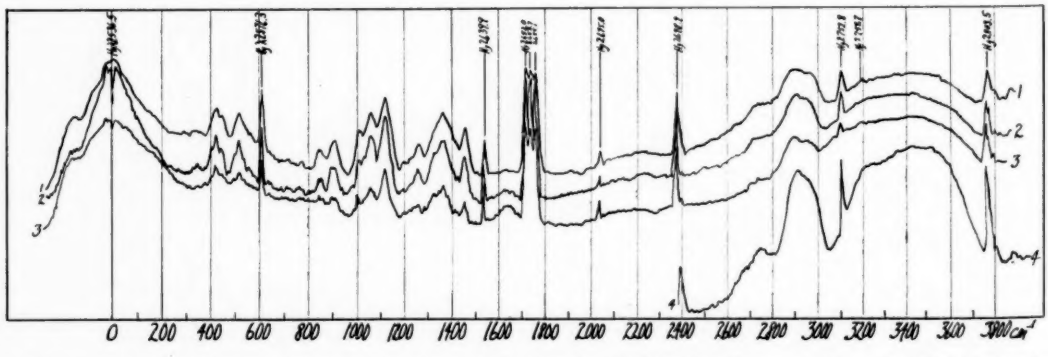

FIG. 3. Superposition of microphotometer tracings of: 1. 5 moles H_2O/mole glucose, 2. 15 moles H_2O/mole glucose, 3. 50 moles H_2O/mole glucose. 4. High λ part of plate with suitable exposure in this region but under-exposed in lower λ region. 5 moles H_2O/mole glucose.

comments until we have obtained much more data on the various sugars. A comparison of the Raman frequencies of anhydrous α- and β-*d*-glucose is given in Fig. 2.

Glucose Solutions

When the sugars are dissolved in water, allowed to come to equilibrium, and the Raman spectra of the solutions obtained, the frequencies are no longer sharp but are broadened considerably. Below 1500 cm^{-1} there are 15 solution bands having no counterpart in the α- or β-form. There are no α-lines which are not covered by a solution band and only two β-lines ($\Delta\nu$ 825 and 1507 cm^{-1}). However, there are four α-lines ($\Delta\nu$ 363, 887, 1057, and 1345) lying more than 5 cm^{-1} from band maxima or shoulders in all three concentrations and five β-lines ($\Delta\nu$ 1051, 1118, 1312, 1363, and 1452) in this category. Unfortunately, the microphotometer available to us was not very satisfactory in that there was a certain amount of random drift in the intensity deflection. While this could be kept at a minimum in closely adjacent regions, absolute intensities or true shapes of lines were not to be depended on except as rough estimates. It is hoped that this microphotometer will be in first class shape in the future as soon as parts can be obtained. In Fig. 3 we have reproduced the microphotometer curves of the three solutions of different concentrations. Within the accuracy of our tracings, which we estimate to be of the order of magnitude of 5 cm^{-1}, there are no systematic changes with dilution except for the frequency 894→899→905. In order to obtain reasonable intensities for the frequencies below 1500 cm^{-1} it is necessary to over-expose the 2800–3600 cm^{-1} region. This has a tendency to flatten the tracing in that range. In curve 4 we have microphotometered a plate (5 moles H_2O/mole glucose) where the 2800–3600 cm^{-1} region was not overexposed.

We do not yet feel justified in drawing any conclusions from the curves as to the percentages of α- and β- (or other) forms present in solution. A careful study of how the frequencies and intensities of the lines shift in going from the anhydrous crystalline forms to the various crystalline hydrates (if they exist) should indicate how the frequencies are affected as the sugar-sugar association is replaced by the sugar-water association. More information should also be obtained by studying the changes in the shape and position of the line envelopes in the equilibrium sugar solutions as the concentration changes from a saturated solution (where considerable sugar-sugar association must still exist) to a very dilute solution (where only sugar-water association could be present). From the above work it can be seen that these shifts must be small, about the order of magnitude of our errors. The question as to whether the difference in the sugar-sugar sugar-water association can cause enough changes in the frequencies and intensities to permit the solution bands to be completely accounted for by the α- and β-forms will have to wait until we have photographed more sugars and their hydrates and have obtained precise microphotometer tracings of their solutions.

The Water Bands

These are located[21] at ~200, 320–1020, 1650, 2167, 3440, and ~4000 cm^{-1}. All of them but the last may be seen in the most dilute *d*-glucose solution (0.1 molar), reproduced in the fifth picture in Fig. 1. Although the water bands in this case cover almost every region except 1000–1500 cm^{-1} it can be seen from this last picture that even in dilute solutions the Raman lines of the sugar can be seen superimposed upon the water bands.

ACKNOWLEDGMENTS

We wish to thank Dr. R. M. Hixon for his interest in and support of this project and the Physics Department for allowing us to use their microphotometer.

[21] Cross, Burnham, and Leighton, J. Am. Chem. Soc. **59**, 1134 (1937).

Vapor Pressures of the Tritium Liquid Hydrogens

Dependence of Hydrogen Vapor Pressure on Mass of the Molecule

W. F. Libby and Cyril A. Barter
Department of Chemistry, University of California, Berkeley, California

(Received December 3, 1941)

The Henry's law constants for HT evaporating from approximately $10^{-9}M$ solutions in normal H_2 and for DT from nD_2 were determined by distillation and measuring the radioactivities of the distillate gases. On the basis of Lewis' and Hanson's data showing H_2 and D_2 to form nearly perfect solutions, the Henry's law constants were taken to represent the vapor pressures of the pure HT and DT liquids. A plot of vapor pressures of various kinds of hydrogen at 20.4°K led to 45±10 mm of Hg as the predicted vapor pressure of liquid nT_2 at 20.4°K.

THE vapor pressures of the hydrogen molecules with tritium (radioactive hydrogen)[1] atoms should help settle certain points in the theory of liquid hydrogen involving the mass and zero-point properties of the liquid. In addition, a distillation technique may prove to be desirable for the concentration of tritium.

The method used consisted principally of the distillation under equilibrium conditions of a small volume of the liquid containing some of the tritium-containing molecules, samples of the gas being taken frequently and their specific radioactivities determined. Under such conditions of no refluxing and perfect stirring of the liquid, the Rayleigh[2] distillation formula applies, with a slight modification due to the large fraction of the hydrogen in the gas phase.

Suppose the vapor pressure of HT over the very dilute solutions (approximately $10^{-9}M$) involved here is given by

$$P_{HT}=\beta N_{HT},$$

where P_{HT} is the pressure and N_{HT} is the mole fraction of HT, and, similarly,

$$P_{H_2}=\alpha N_{H_2}=\alpha(1-N_{HT}).$$

Then the specific radioactivity or mole fraction of HT of the distillate gas ρ will be given by

$$\rho=\rho_0\left(\frac{1+(\alpha/\beta)v_0/V}{1+(\alpha/\beta)v/V}\right)^{(\alpha-\beta)/\alpha},$$

where V is the volume of the gas space over the liquid and v_0 and v are the volumes of the liquid at the beginning of the distillation and at any subsequent point, measured in terms of the volumes of gas to which they are equivalent.

To derive this expression one notes that the total number of moles of HT in the distillation vessel is

$$t=\rho V+\rho(\alpha/\beta)v,$$

since ρ is the mole fraction of HT in the gas and is equal to $(\beta/\alpha)N_{HT}$.

For a small removal of gas from the distillation chamber, changing v by dv,

$$dt=Vd\rho+(\alpha/\beta)\rho dv+(\alpha/\beta)vd\rho$$

or, after dividing by dv and replacing dt/dv by ρ,

$$\rho=(V+(\alpha/\beta)v)d\rho/dv+\alpha/\beta\rho.$$

Rearranging gives

$$(\beta/\alpha-1)d\ln(V+(\alpha/\beta)v)=d\ln\rho,$$

since V is essentially constant. Finally, integration gives the equation desired. Figure 1 illustrates the expected course of the specific activity

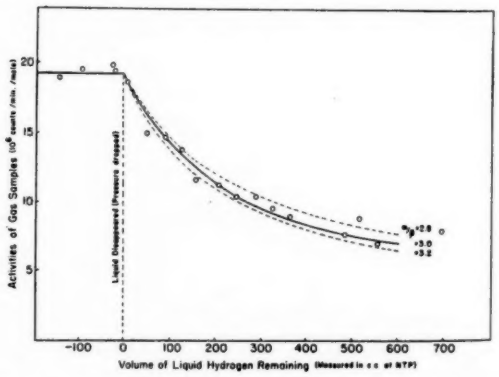

FIG. 1. Activity distillation curve for HT from nH_2 (20.4°K). Solid line: calculated curve for pressure ratio of 1 to 3.0.

[1] Luis W. Alvarez and Robert Cornog, Phys. Rev. **56**, 613 (1939).
[2] Lord Rayleigh, Phil. Mag. [5] **4**, 527 (1902).

for the case where V was 500 cc (measured at 295°K and one atmosphere) and α/β was 3.0.

The distillation bulb was immersed deeply in a bath of boiling normal H_2 and the previously prepared radioactive gas introduced with a Toepler pump through several feet of small bore (1 mm) capillary glass and copper tubing. After a few minutes, gas was slowly withdrawn at equilibrium pressure into a series of bulbs which were stored for later measurement of their radioactivities. The total volume of gas used varied between one and five liters NTP and the sample bulbs were mainly of 25 cc and 100 cc capacities, the smaller bulbs being used near the point of disappearance of the last of the liquid. Obviously under the conditions outlined refluxing of the distillate is quite impossible. The second condition, that the liquid be in equilibrium with the vapor, is less easily established. Indeed, for the run shown in Fig. 1 some five liters of gas were used and only the last liter distilled under equilibrium conditions as attested by the agreement between the points and the calculated curve. The result is understandable when one realizes that the vessel in which the gas and liquid came to equilibrium was about 2

TABLE I.

Molecule	Vapor pressure at 20.4°K (mm Hg)	Source
H_2	760	
HD	438	Reference 1.
D_2	256	References 2–5.
HT	254±16	This research.
DT	123±6	This research.
T_2	(45±10)	Extrapolation, Fig. 3.

[1] R. B. Scott and F. G. Brickwedde, Phys. Rev. **48**, 483 (1935).
[2] R. B. Scott, F. G. Brickwedde, H. C. Urey, and M. H. Wahl, J. Phys. Chem. **2**, 454 (1934).
[3] K. Clusius and E. Bartholomé, Zeits. f. physik. Chemie **B30**, 237 (1935).
[4] E. Bartholomé, Zeits. f. physik. Chemie **B33**, 387 (1936).
[5] H. D. Megaw and F. Simon, Nature **138**, 244 (1936).

square cm² in cross-sectional area and about 15 cm long. Five cc of liquid hydrogen created quite a distance for diffusion to accomplish stirring. Fortunately, diffusion was sufficiently rapid when the liquid volume was reduced.

Figure 2 presents similar data for distillation of DT out of $n D_2$. In this case the bulb size was somewhat greater, reducing the number of points. However, the larger size of the bulbs increased the accuracy of the counting because the 500 cc

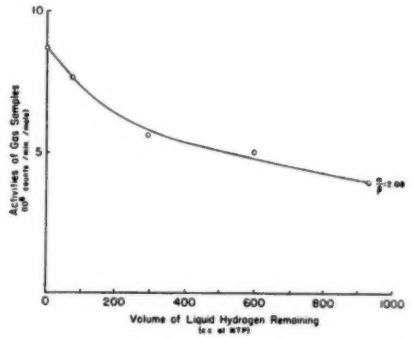

FIG. 2. Activity distillation curve for DT from $n D_2$ (20.4°K). Solid line: calculated curve for pressure ratio of 1 to 2.08.

counter used could be filled several times to the 2 cm of Hg pressure used. The point placed just at the point of disappearance of the liquid was obtained by using the activity of the gas present after the liquid had disappeared. The gas volume V was 550 cc in this run.

The HT samples were prepared by allowing Li metal which had been irradiated for several months by the Berkeley cyclotron (the authors are indebted to the Radiation Laboratory and Dr. Robert Cornog for this irradiation) to react with H_2O after all air had been removed by pumping on the liquid-air-cooled reaction mixture. The appropriate amount of Li metal was cut from the irradiated block and placed in a liquid-air-cooled tube containing sufficient water as ice. The tube was then placed on the vacuum line and pumped. The vessel then warmed to room temperature and evolved H_2. The gas was passed through liquid-air traps for water removal. The procedure for DT was identical, except that D_2O was used instead of H_2O for reaction with the lithium. The gases were stored in large bulbs and transferred with a Toepler pump to the distillation cells. The purity of the gases must have been high because the capillary tubing immersed in liquid H_2 for about two feet would have plugged immediately with any air, water vapor or any gas except the lightest rare gases. In addition the H_2 and D_2 samples gave the vapor pressures reported in the literature.

Two entirely separate runs were made with HT. The first one gave a value for α/β of 3.3±.5 considerably less accurate than the one described above, but in definite agreement with it. There seem to be only two likely sources of

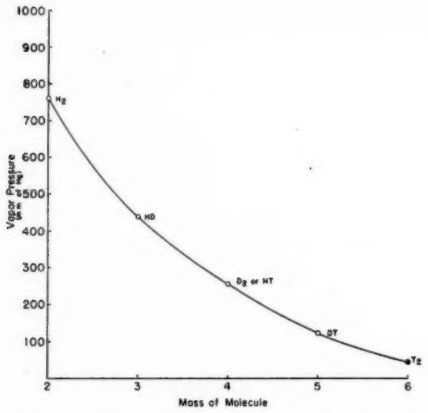

FIG. 3. Plot of vapor pressures of hydrogen molecules *versus* mass, at 20.4°K.

error in this type of experiment. The first is the condition that diffusion equilibrium exist and the second is that the samples of gas have their radioactivities measured properly. In connection with the first point, one notices on Fig. 1 that there remained only 600 cc of hydrogen as liquid when the data were considered to represent safely equilibrium distillation. When one realizes that this amounts to about $\frac{1}{2}$ cc of liquid hydrogen in the distillation cell or a layer of liquid hydrogen approximately $\frac{1}{4}$ cc thick over the 2 cm^2 bottom of the cell, it is difficult to imagine any but equilibrium conditions applying after 10 minutes, which was the average interval between samples.

The gaseous samples were counted by filling the counter with approximately 1.5 cm of Hg of H_2 or D_2 and 2 or 3 mm of Hg of ethyl alcohol vapor. A standard uranium sample was used to check the reproducibility of the counting apparatus. In connection with the accuracy of the counting, it was observed that air had not entered the sample bulbs and that the gas composition was uniform by noting the operating voltage for the counter when filled with the various samples. Counters are very sensitive in this respect. This being so, one could feel certain that the counter's sensitivity to tritium radiation would be reproduced if its sensitivity to uranium were reproduced.

The figures quoted for the errors in the values of the vapor pressures were obtained as shown in Fig. 1 by sketching in the curves for values of α/β such that most of the points were included between the limits. The values for V were obtained by measurement of the cell volume and correcting to 20.4°K.

Table I summarizes the results for the vapor pressures of the hydrogen molecules at 20.4°K.

In compiling the data the Henry's law constants β obtained for the very dilute solutions were assumed to represent the true vapor pressure of the pure solute, i.e., the solutions were assumed to be perfect. Evidence for the essential correctness of this assumption exists in the data on the vapor pressures of H_2, D_2 solutions.[3]

The first point the data emphasize is that the vapor pressure of HT is essentially the same as that for normal D_2. This is rather to be expected when one realizes that the difference in moment of inertia can have little effect so long as nearly free rotation occurs in the liquid, a condition fairly well substantiated by specific heat data on H_2.

The second point is shown in Fig. 3 where the vapor pressures of the various hydrogen molecules are plotted against their masses, the value for T_2 being obtained by extrapolation of the curve. Very evidently, the distillation technique should be successful in concentrating tritium if one were to keep the equilibria

$$2HT = T_2 + H_2$$

and

$$2DT = T_2 + D_2$$

well catalyzed by periodically passing the gas over a heated catalyst in the last stages of the concentration.

The complete significance of the curve in Fig. 3 must await a successful theory of liquid hydrogen. However, qualitatively it reveals the effect of translational zero-point energy on the free energy of the liquid. The van der Waals forces holding the liquids together will be nearly identical for all the liquid hydrogens. Therefore one must expect the mass effect observed to be associated very directly with the differences of the zero-point energies of the compressional vibrations of the several liquids. The effects due to rotation certainly are small compared with these mass effects. In addition they are averaged out somewhat in the data chosen for Fig. 3.

[3] Gilbert N. Lewis and W. T. Hanson, Jr., J. Am. Chem. Soc. **56**, 1000 (1934).

Solid Solutions of the Alkali Halides

ARTHUR V. TOBOLSKY
Albert Plaut Fellow in Chemistry, Princeton University, Princeton, New Jersey
(Received December 18, 1941)

X-ray studies of solid solutions of alkali halide pairs with a common ion at room temperature and at 550°C show that these pairs can be divided into three groups depending on the percent deviation δ of their lattice parameters. For values of δ less than 6 percent miscibility is complete at room temperature. For values of δ between 6 and 13 percent miscibility is complete at 550°C. For values of δ larger than about 13 percent miscibility is not complete at 550°C. In terms of the Born theory of ionic lattices, the free energy of mixing, and Vegard's law, an approximate theory for the phase curve of these solid solutions is derived. For a typical alkali halide with an electrostatic energy of 180 kcal. at the absolute zero of temperature the equation of the phase curve is

$$9\delta^2/T(1-2x)+\ln x-\ln(1-x)=0,$$

where x is the mole fraction of one component dissolved in the other. The temperature above which miscibility is complete is given by $T=4.5\delta^2$. The heat of mixing is approximately $-9\delta^2$ cal. The predictions of this theory are in good agreement with the above-mentioned experimental observations.

SOLID SOLUTIONS OF THE ALKALI HALIDES

IT has long been known that when certain mixtures of alkali halides with a common ion are brought into contact solid solution formation takes place.[1] Only recently, however, has the rate of attainment of equilibrium for this solid solution formation been carefully studied.[2] It has been found that at room temperature if the salt mixtures are kept dry, it will take a matter of several weeks for equilibrium to be reached. The presence of moisture will cut the time to one day. At high temperatures if the salt mixtures are fused, quickly quenched, then ground in an agate mortar and annealed in a Victor Meyer furnace at 550°C, it will take only a few hours for equilibrium to be reached.

Continuing the work of Matsen and Beach in this laboratory, a study was made to determine what are the stable phases when equimolal mixtures of alkali halide pairs with a common ion are brought together at room temperature and at 550°C. In general, each component is somewhat soluble in the other and two solid solution phases occur. The extent of solution is greater if the lattice parameters are more nearly equal, and the amount of solubility increases with the temperature. For certain mixtures for which the lattice parameters are nearly equal miscibility is complete at room temperature and a single phase will result when equilibrium is reached. For others, for which the percent difference between the lattice constants is somewhat larger two phases result at room temperature but miscibility is complete at 550°C. For a third class of these mixtures for which the lattice parameters are widely different the solubility will be small and two phases will result for all temperatures below the melting temperature.

The method used in this study to determine the equilibrium phases is an x-ray powder method fully described in the paper by Matsen and Beach. No attempt was made to determine quantitatively the composition of the phases, but merely to determine whether or not miscibility was complete. In most cases where it was found that two phases were formed, these phases were found to be nearly pure phases on the criterion that their lattice constants were not much different from the lattice parameters of the pure phases. A similar study had previously been made by the x-ray method for some of these mixtures at room temperature.[3] Attempts to determine the width of the miscibility gap of the phase diagram had also been made by other methods.[1] The various results have been collected

[1] For a general review see Bruni, Chem. Rev. **1**, 345–375 (1924).
[2] Matsen and Beach, J. Am. Chem. Soc. **63**, 3470–3473 (1941).
[3] Havighurst, Mack, and Blake, J. Am. Chem. Soc. **47**, pp. 29–43.

TABLE I.

Alkali halide pairs	δ	Equilibrium conditions: this study	Remarks from other studies
NaF-KF	15.4	15°C Two nearly pure phases* 550°C Two nearly pure phases	
NaCl-KCl	11.5	15°C Two nearly pure phases 550°C Complete miscibility	H.M.B.:† Solution of a few percent KCl in NaCl Bruni:‡ Mixed crystals formed from melt destroyed at room temperature
NaBr-KBr	10.8	15°C Two phases 550°C Complete miscibility	Bruni: Mixed crystals formed from melt destroyed at room temperature
NaI-KI	9.1	15°C Two phases 550°C Completely miscible	H.M.B.: Very low solubility at room temperature Bruni: Mixed crystals formed from melt destroyed at room temperature
NaF-NaI	39.8	15°C Two nearly pure phases 550°C Two nearly pure phases	
NaCl-NaBr		15°C Complete miscibility 550°C Complete miscibility	Studied by many investigators
NaBr-NaI	8.8	15°C The x-ray lines could not be interpreted 550°C Complete miscibility	
KF-KCl	17.8	15°C Two nearly pure phases 550°C Two nearly pure phases	
KF-KBr	23.5	15°C Two nearly pure phases 550°C Two nearly pure phases	
KF-KI	32.3	550°C Believed to be two nearly pure phases. KF lines do not show very well	
KCl-KBr	4.8	15°C Completely miscible 550°C Completely miscible	
KCl-KI	12.3	15°C Slight dissolving of KCl in KI 550°C More extensive dissolving ing of KCl in KI but not completely miscible	Bruni: At room temperature the miscibility gap extends from 7–90%. Near the melting temperature the miscibility gap is between 49 and 91%
KBr-KI	7.1	15°C Two phases 550°C Completely miscible	H.M.B.: KBr soluble to the extent of 15 or 20% in KI at room temperature Bruni: Miscibility gap between 34 and 93%

* By this phrase we mean that the x-ray picture shows two phases that differ very slightly from the pure components.
† Reference 3, Havighurst, Mack, and Blake.
‡ Reference 1. Within the approximations of the theory to be developed $100(a_2-a_1)/a_1=100(a_2-a_1)/a_2=100(a_2-a_1)/[(a_1+a_2)/2]=\delta$, so that it does not matter which particular definition we adopt for purposes of tabulation.

in Table I. The quantity δ that appears in this table is the percent deviation between the lattice constants a_1 and a_2 of the component salts.

It will be seen, as had been noted previously,[3] that for salt mixtures for which the value of δ is less than 5 or 6 percent miscibility is complete at room temperature. Working under the supervision of Dr. Beach in this laboratory I have made further x-ray studies at high temperatures and noted that for values of δ between approximately 6 percent and 13 percent miscibility is partial at room temperature and complete at 550°C (i.e. only one phase is observed in the x-ray powder photograph). For larger values of δ two phases are always observed and especially at room temperature the phases are very nearly the original pure components.

In order to explain these phenomena, I have developed a theory for the phase diagram of these salt mixtures in terms of the Born theory for ionic lattices, Vegard's law, and the free energy of mixing. It is commonly accepted that in a solid solution such as KCl-KBr the Cl^- ions substitute for Br^- ions at random in the KBr lattice. Superstructure lines which characterize ordered lattices such as occur in many alloys have never been observed for mixed crystals of alkali halides. One must therefore assume that if there is any ordering phenomena the Curie point for order-disorder occurs far below room temperature. In this theory it has been assumed that the substitution is perfectly random at all temperatures, i.e. whatever mixed crystals occur are perfect mixed crystals.

A general expression for the lattice parameter of a solid solution in terms of the parameters of the components has been suggested to be of the form

$$a^n=a_1^n+(a_2^n-a_1^n)x,$$

where x is the mole fraction of component 2 in the solid solution and n is a constant to be empirically determined.

The special case where $n=1$ is known as Vegard's law. This law has been found to hold true for a large number of solid solutions. Values of $n=3$ and $n=8$ have also been proposed. The latter value of $n=8$ has been proposed as a result of a theoretical study by Grimm and Herzfeld but has not been verified experimentally. The previously mentioned study of Havighurst, Mack, and Blake has shown that for values of δ less than 6 percent solid solutions of the alkali halides at room temperature obey Vegard's law rather closely. It is, however, hard to distinguish experimentally between the values $n=3$ and $n=1$ for these particular solid solutions. For simplicity in the theoretical derivation of the phase diagram, I have assumed the validity of Vegard's law.

By far the largest portion of the energy of an alkali halide is given by the Born evaluation of the electrostatic energy of the crystal lattice which is

$$U_{00}=(NAe^2z^2/a_0)(1-1/m),^4$$

where N = Avogadro's law number, e = electronic charge, z = charge on ion, a_0 = distance from any ion to nearest neighbor, A = Madelung constant.

The term in $-1/m$ represents the repulsive energy of the lattice, where m is approximately 8. If we collect all the terms in the numerator of the above expression and call them M, we have $U_{00}=-M/a_0$.

The U_{00} represents by far the largest contribution to the energy of the ionic crystal lattice. Various other contributions such as van der Waal's energy, polarization energy, etc., range from 1 to 5 percent as is seen from the values of U_0 and U for the alkali halides listed in Table II. U represents the total energy of the lattice[5] (not including thermal energy which is given by a Debye term).

The heat of formation of these solid solutions is in general endothermic, i.e., their formation absorbs heat. This is in accordance with the fact that solubility in the solid state increases with temperature. Also it is experimentally observed that the heat changes are greatest in the pairs KCl-NaCl, KBr-NaBr, KI-NaI whose mixed crystals are formed at high temperatures but are unstable at room temperature. Then comes KCl KI which has a large miscibility gap at room temperature, but at high temperature has a small miscibility gap. The heat of formation of the solid solution of KBr-KI is somewhat less; the miscibility which is complete just below melting shows at 25°C a gap between 34 and 93 percent. Finally, the smallest heat of formation within the series is shown by KCl-KBr where solubility in the solid state is complete at room temperature.[6]

If we assume the validity of Vegard's law, we can make an approximate calculation of these heats of formation. The energy U_{00} of an equi-

TABLE II.‡

	$-U_0$ (Sherman)	$-U$ calculated (Mayer)	$-U$ experimental (Sherman)
Li F	240.1	242.0	
Li Cl	193.3	200.2	198.1
Li Br	183.1	189.7	189.3
Li I	170.7	176.2	181.1
Na F	215.0	214.5	
Na Cl	180.4	184.4	182.8
Na Br	171.7	176.5	173.3
Na I	160.8	166.1	166.4
K F	190.4	191.8	
K Cl	164.4	167.5	164.4
K Br	157.8	161.7	156.2
K I	149.0	153.1	151.5
Rb F	181.8	184.2	
Rb Cl	158.9	162.7	160.5
Rb Br	152.5	156.7	153.3
Rb I	144.2	148.4	149.0
Cs F	172.8	175.8	
Cs Cl	148.9	155.6	155.1
Cs Br	143.5	150.0	148.6
Cs I	136.1	142.7	145.3

‡ See reference 5.
U_0 is calculated from the Born theory described above using values of m that are determined by use of experimental values of the compressibility and generally lie in the vicinity of 9. The lattice parameter used is that measured at room temperature and therefore U_0 is slightly different from U_{00} because of thermal expansion. Mayer's more accurate calculations involve the use of an exponential term for the repulsive energy and also includes van der Waals energy.

[4] U_{00} is the electrostatic energy of the lattice at the absolute zero of temperature.

[5] See Seitz, *Modern Theory of Solids*, Chapter 2. The more penetrating analysis of Mayer in which an exponential law for repulsion between the ions is used does not alter the results sufficiently to warrant its use in the approximations here used.

[6] The foregoing remarks on heats of formation of these solid solutions are adapted from reference 1 as are the experimental data cited in Table III.

molal solid solution is given by

$$U_{00} = -M/[(a_1+a_2)/2].^{7}$$

Let us take for example the reaction KCl+KBr = (solid solution KCl, KBr). (a_1 and a_2 are here the lattice parameters of the pure components which form the solid solution.)

$$\Delta H = -\frac{2M}{(a_1+a_2)/2} + \left(\frac{M}{a_1}+\frac{M}{a_2}\right)$$

$$\Delta H = M\left(\frac{-4a_1a_2+a_2(a_1+a_2)+a_1(a_1+a_2)}{(a_1+a_2)(a_1a_2)}\right)$$

$$= \frac{M(a_1-a_2)^2}{(a_1+a_2)(a_1a_2)} \leqq \frac{M}{2a}\frac{\delta^2}{10000}$$

approximately $\Delta H \leqq 9\delta^2$ since $M/a \sim 180{,}000$ cal. (a is a kind of average between a_1 and a_2).

We have therefore an approximate evaluation of the heats of formation of these solid solutions in terms of the deviation

$$\frac{\delta}{100} = \frac{a_2-a_1}{(a_2+a_1)/2}.$$

In the above derivation we have used the fact that $M/a = -U_0$ is on the average 180,000 calories for the alkali halides. In Table III we have compiled the experimental and the calculated values for the heats of formation of some of these solid solutions. It is only in the cases where Vegard's law is obeyed and the miscibility is complete, i.e., cases where δ is smaller than 6 percent that we can expect heats of formation measured at room temperature to check the calculated values.

TABLE III.

System	δ	ΔH (calculated) in calories	ΔH (observed) in calories
KCl-RbCl	4.53	166	203
KBr-KCl	4.8	187	220
NaCl-NaBr	5.5	236	——
KBr-KI	7.1	389	(390)
NaI-KI	9.1	646	(1250)
NaBr-KBr	10.8	960	(1400)
NaCl-KCl	11.5	1188	(2150)

The numbers enclosed in parenthesis are unreliable because the equimolal solid solutions of the corresponding systems are unstable at room temperature. Since ΔH is obtained by measuring heats of solution in water this necessitates using quenched solid solutions which are of course thermodynamically unstable.

In order to derive the phase curve for these solutions we consider the question: Suppose we mix in equimolal proportions two alkali halides, of lattice parameters a_2 and a_1, with $a_2 \geq a_1$. If we allow the mixture to come to equilibrium the general result will be two phases, a solid solution of component 1 in component 2, and a solid solution of component 2 in component 1. It is a consequence of the assumptions and approximations of this theory that the amount of component 2 in component 1 is equal to the amount of component 1 dissolved in component 2. This does not alter the general shape of the phase diagram and for simplicity we shall first derive the phase curve on this basis. We shall later discuss this question more fully from a theoretical standpoint and compare with experimental observations.

The total Gibbs free energy for one mole of alkali halide crystal is $U+A_d+pV=F$. U is the electrostatic energy of the crystal.[8] If we neglect expansion of the crystal, $U=U_{00}$. A_d represents the Debye expression for the Helmholtz free energy. pV is negligibly small below the melting point.

Since a large portion of the free energy is comprised by the term U_{00}, and since the Debye temperatures and the extra electrostatic energies of expansion of the alkali halides are all of the same order of magnitude, we shall assume that insofar as it has any effect on the process of mixing $F=U_{00}$.

Now let us suppose that we mixed two alkali halide crystals (one mole of each). The free energy of the two solid solution phases formed is

$$F = -\left(\frac{M}{a'}+\frac{M}{a''}\right) + 2RT\{x\ln x + (1-x)\ln(1-x)\}$$

where x is the mole fraction of component 1 in the one solid solution phase or the mole fraction

[7] Actually we should here use

$$H = \frac{U_{00}}{1-1/m}\left[\frac{a_0}{a} - \frac{1}{m}\left(\frac{a_0}{a}\right)^m\right] + \frac{9}{8}R\theta + RD\left(\frac{\theta}{T}\right) + pv$$

for the heat content of one mole of alkali halide crystal. But this is not very different from U_{00} and we are using the latter as a good approximation. The heat of reaction is of course $-\Delta H$. ($9R\theta/8+RD(\theta/T)$ represents Debye energy.) a_0 represents the lattice parameter of absolute zero, a the lattice parameter at temperature in question.

[8] For a complete discussion see Slater, *Introduction to Chemical Physics*, Chaps. 23 and 13.

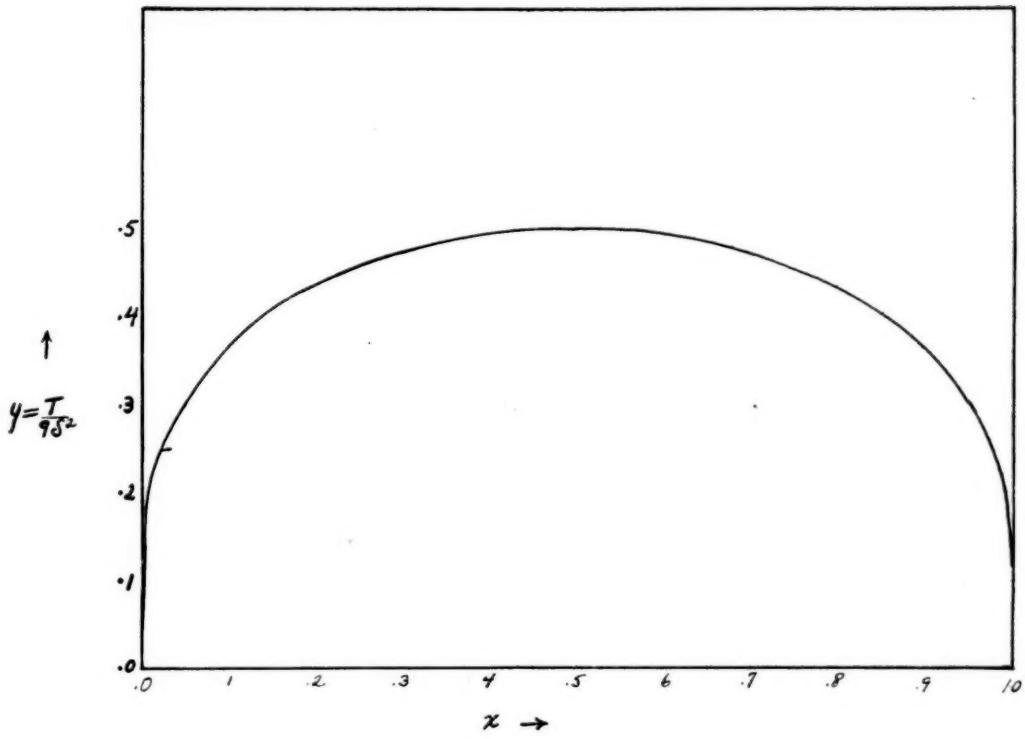

FIG. 1.

of component 2 in the other solid solution phase and where a' is the new lattice parameter of the first solid solution phase and a'' is the lattice parameter of the second solid solution phase. By Vegard's rule

$$a' = a_1 + (a_2 - a_1)x,$$
$$a'' = a_2 + (a_1 - a_2)x.$$

Using these values

$$F = -\frac{M}{a_1 + (a_2 - a_1)x} - \frac{M}{a_2 + (a_1 - a_2)x} + 2RT\{x \ln x + (1-x) \ln (1-x)\}.$$

In order to determine x we wish the free energy to be a minimum. After carrying through a little algebra we can find x as a function of T and δ the percent deviation of the two lattice parameters.

$$\frac{\partial F}{\partial x} = 0 = \frac{M(a_2 - a_1)}{[a_1 + (a_2 - a_1)x]^2} + \frac{M(a_1 - a_2)}{[a_2 + (a_1 - a_2)x]^2} + 2RT(\ln x - \ln (1-x)) = 0. \quad (1)$$

$$\frac{\frac{M}{a_1}\frac{a_2 - a_1}{a_1}}{\left[1 + \left(\frac{a_2 - a_1}{a_1}\right)x\right]^2} - \frac{\frac{M}{a_2}\frac{a_2 - a_1}{a_2}}{\left[1 - \left(\frac{a_2 - a_1}{a_2}\right)x\right]^2} + 2RT[\ln x - \ln (1-x)] = 0. \quad (2)$$

Let us put

$$\delta_1 = \frac{a_2 - a_1}{a_1}, \quad \delta_2 = \frac{a_2 - a_1}{a_2},$$

$$0 = \frac{M}{a_1}\frac{\delta_1}{(1 + \delta_1 x)^2} - \frac{M}{a_2}\frac{\delta_2}{(1 - \delta_2 x)^2} + 2RT[\ln x - \ln (1-x)]. \quad (3)$$

Since $\delta_1 \leqq \delta_2 \leqq 0.05$; $x \leq 1$ we can expand by binomial theorem.

$$0 = M(a_2 - a_1)\left[\frac{1}{a_1^2} - \frac{1}{a_2^2}\right] - \frac{2M(a_2 - a_1)^2}{a_1^3}x - \frac{2M(a_2 - a_1)^2}{a_2^3}x + 2RT[\ln x - \ln (1-x)], \quad (4)$$

$$0=\frac{M(a_2-a_1)^2(a_2+a_1)}{a_1^2a_2^2}-\frac{2M}{a_1}\left(\frac{a_2-a_1}{a_1}\right)^2x$$

$$-\frac{2M}{a_2}\left[\frac{a_2-a_1}{a_2}\right]^2x+2RT[\ln x-\ln(1-x)]. \quad (5)$$

$$2M(a_2-a_1)^2/a^3(1-2x)$$

$$+2RT[\ln x-\ln(1-x)]=0. \quad (6)$$

(a is a kind of average between a_1 and a_2.) For the alkali halides we have seen that the average value of U_{00} is 180,000 cal. For the purpose of obtaining a general equation suitable for all alkali halides we set

$$M/a\sim 180{,}000 \text{ cal.}, \quad R=2 \text{ cal./degree},$$

$$\delta=100(a_2-a_1)/a.$$

Hence $9\delta^2/T(1-2x)+\ln x-\ln(1-x)=0$. We let

$$y=\frac{T}{9\delta^2}, \quad y=1-2x\Big/\left[\ln\left(\frac{1-x}{x}\right)\right],$$

$$y_{\text{maximum}}=\tfrac{1}{2}.$$

We can make a table of y against x. See Table IV.

The graph (Fig. 1) shows a plot of the mole fraction dissolved against $T/9\delta^2$. The characteristic feature of the curve is that it rises very steeply near the axis of zero concentration and then rounds off to reach a maximum beyond which miscibility is complete. The critical mixing temperature for various values of δ is given in Table V. It is seen that this theory predicts complete miscibility at room temperature for values of δ less than 8 percent as compared with the value of 5 or 6 percent that would be expected on the basis of experiment. At higher temperatures the theory is in accord with the experimental data obtained so far. The initial steepness of the curve explains why many mixtures completely miscible at high temperatures give at room temperature an x-ray photograph in which the two phases appear nearly pure.

TABLE IV.

x	0.01	0.02	0.05	0.10	0.20	0.30	0.40	0.50
y	0.2175	0.2473	0.3004	0.3640	0.4329	0.4723	0.4938	0.5000

TABLE V.

δ	Critical mixing temperature	δ	Critical mixing temperature
1	4.5° Abs.	10	450.0° Abs.
2	18.0	11	544.5
3	40.5	12	648.0
4	72.0	13	760.5
5	112.5	14	882.0
6	162.0	15	1012.5
7	220.5	16	1152.0
8	288.0	17	1300.5
9	364.5	18	1458.0
		19	1714.5

It is a consequence of the approximations of this theory that the mole fraction of component 1 dissolved in component 2 is equal to the whole fraction of component 2 dissolved in component 1. This can be seen by assuming that a certain amount x of component 1 is in solid solution 1 and a certain amount y of component 2 is in solid solution 1. The composition of the other solid solution phase (solid solution 2) is then determined by the original amounts of the pure components. By equating the partial potentials of each component in the two phases we find that if we start out with equal amounts of the two pure components, x will be equal to y. The partial free energies are of course obtained by setting up the expressions for the total free energy of each phase according to the same approximations used above and differentiating with respect to the amount of component in the phase. The consequence that $x=y$ is not borne out by experiment, but the general shape of the phase curve should not be radically wrong because of this error.

Letters to the Editor

THIS section will accept reports of new work, provided these are terse and contain few figures, and especially few halftone cuts. The Editorial Board will not hold itself responsible for opinions expressed by the correspondents. Contributions to this section should not exceed 600 words in length and must reach the office of the Managing Editor not later than the 15th of the month preceding that of the issue in which the letter is to appear. No proof will be sent to the authors. The usual publication charge ($3.00 per page) will not be made and no reprints will be furnished free.

The Thermal Reaction Between Hydrogen and Oxygen at Higher Pressures

O. OLDENBERG AND H. S. SOMMERS, JR.
Research Laboratory of Physics, Harvard University, Cambridge Massachusetts
January 27, 1942

IN recent experiments we found conditions under which the thermal hydrogen-oxygen reaction ($p=60$ cm; T up to 560°C) is sufficiently reproducible so that the temperature dependence of the rate could be measured. From the constant activation energy observed over a certain temperature range, we inferred that here the reaction proceeds in non-branched chains. In a recent letter to the editor, Dainton[1] concludes that the chains are branched. From an enlargement of our pressure-time curve representing a typical reaction, he concludes that at the beginning the first derivative of the rate $(\delta^2(\Delta p)/\delta t^2)$ is increasing and that the plot of $\log \Delta p$ against time is linear; applying Semenoff's theory, he argues that in the first stages of the reaction branching of the chains is occurring and, in fact, more frequently than their termination.

This conclusion seems questionable for the following reasons. The beginning of our curve analyzed by Dainton is not reproducible enough to apply Semenoff's criterion; in many cases $\delta^2(\Delta p)/\delta t^2$ seems to begin with its largest value; in still more cases (old vessel) the reaction begins with nearly the maximum rate. The reproducibility of the maximum rate (or rather log rate), however, is evident from our curves (reference 1, Figs. 2–5).

Moreover, immediately after high evacuation near the annealing temperature of Pyrex and subsequent admission of almost one atmosphere of gases, one should expect rapid changes of the surface by adsorption superimposed on the effects considered by Semenoff. This difficulty may be less pronounced in the low pressure explosion (Kowalsky, pressure a few mm, reaction lasting a small fraction of a second); this reaction, which is quantitatively described by Semenoff's theory, takes place under conditions so widely different from those at high pressure that Hinshelwood and Williamson even postulated a mechanism of a different nature.[2] Whether the high pressure reaction should actually be interpreted by Semenoff's theory can possibly be determined by a photochemical investigation; if the induction period is correlated with the time required for the development of a chain, a corresponding *decay period* should be observed after the interruption of the illumination. Taylor and Salley, in their photochemical investigation, mention the induction period but not such a decay period.

There is another difficulty in Dainton's interpretation. He assumes that in the beginning of the reaction the branching exceeds the breaking and the explosion is prevented by the change of concentrations occurring during the development of the first chains. He argues that the maximum rate occurs when $\phi=0(\delta-\beta=0)$ and that in this region the chains are of constant finite length. While we are unable to find a proof for this general theorem, it seems to us that the condition for the maximum rate would largely depend on the detail of the reaction. In the case thoroughly treated by Semenoff,[3] "the velocity of the reaction begins to decrease long before $\delta-\beta$ becomes equal to 0."

We applied the conventional procedure (Hinshelwood and Thompson, Taylor and Salley, and Prettre), measuring the nearly constant rate after the induction period. This seems justified in the limiting case of an initial rate which nearly equals and rapidly reaches the maximum rate (many observations in Pyrex, Prettre's observations in the KCl covered vessel); here one should be able to derive an activation energy from the temperature coefficient of the maximum rate. The same procedure leads to well-defined values of the activation energy for various kinds of surface yielding short or long induction periods. Therefore, we consider our interpretation of our curves most plausible, although not inevitable. This procedure does not involve an assumption regarding the nature of the induction period. In order to explore the effects of a pretreatment of the walls and of impurities on this period, we started experiments a year ago which are now interrupted.

[1] F. S. Dainton, J. Chem. Phys. **9**, 826 (1941); see F. S. Dainton and R. G. W. Norrish, Proc. Roy. Soc. **A177**, 393 (1941). For further references see Dainton's paper and our paper, J. Chem. Phys. **9**, 432 (1941).
[2] C. N. Hinshelwood and A. T. Williamson, *The Reaction between Hydrogen and Oxygen* (Clarendon Press, Oxford, 1934), p. 52.
[3] N. Semenoff, *Chemical Kinetics and Chain Reactions*, p. 62.

The Infra-Red Absorption of $C^{13}O^{16}$ at 4.66 Microns

R. T. LAGEMANN*
Mendenhall Laboratory of Physics, The Ohio State University, Columbus, Ohio
January 23, 1942

AFTER taking the necessary experimental precautions, it has been found possible to find rotational lines due to the isotopic carbon monoxide molecule $C^{13}O^{16}$. These lines are found interspersed among the lines of the fundamental band of $C^{12}O^{16}$ at 4.66 microns.

A portion of the absorption curve is shown in Fig. 1. The more intense lines are due to the $C^{12}O^{16}$ molecule. The weaker lines are associated with the $C^{13}O^{16}$ molecule, and comprise part of the R branch of that molecule's fundamental band. At lower frequencies than are shown here the isotopic lines become relatively more intense. As is to be expected, the line spacing for the heavier isotope is less than that for the lighter one.

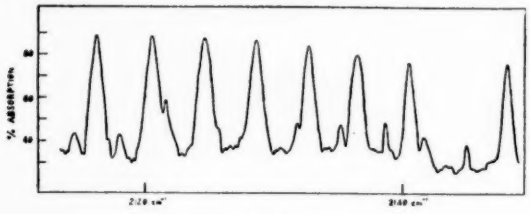

FIG. 1.

The grating used was an echelette replica of 2887 lines per inch, ruled for the region 9 to 12 mu and employed in the second order. Readings of percent absorption were made at intervals of 5 seconds of arc, equivalent to about 0.13 cm^{-1}. The slit width was equivalent to 0.22 cm^{-1}.

Measurements are soon to be made on the overtone band and a complete report will be made at a later date.

* Emory University, Emory University, Georgia.

The Vibrational Structure of Electronic Transitions for Some Complex Ions

MELVIN L. SCHULTZ
Department of Chemistry, Illinois Institute of Technology, Chicago, Illinois
February 9, 1942

FOR several compounds of some of the transition elements, absorption spectra consisting of groups of approximately equidistant bands have been reported. The positions of the bands and the intervals between them depend only upon the metal ion and upon the identity of the complex of which the metal ion is a part. These spectra may be interpreted as originating in electronic transitions in which the vibrational structure characteristic of the complex ion present is resolved. The experimental basis for this interpretation is summarized in the following paragraphs.

Dreisch and Trommer[1] have found in dilute aqueous solutions of $CoCl_2$, $CoBr_2$ and CoI_2 an absorption band at 1.23μ consisting of six maxima with an average separation of 248 cm^{-1}. This band may be attributed to the $Co(OH_2)_6^{++}$ ion. In aqueous solutions of $NiCl_2$, $NiSO_4$ and $Ni(NO_3)_2$ they have found at 1.17μ a band characteristic of the $Ni(OH_2)_6^{++}$ ion. This band is resolved into four maxima with a separation of 264 cm^{-1}. In ammoniacal solutions of $Ni(NH_3)_6Cl_2$ the band is shifted to 0.940μ and the separation becomes 390 cm^{-1}, the number of maxima remaining the same. For solutions of a number of ferrous salts, Dreisch and Kallscheuer[2] have reported a series of twelve or thirteen bands extending from about 0.7μ to about 1.27μ. The intervals separating the five bands of highest frequency vary considerably from salt to salt. The separations of the next seven bands are approximately the same for all of the salts measured. This constant separation, 324 cm^{-1}, is then characteristic of the $Fe(OH_2)_6^{++}$ ion.

The absorption spectra, measured at liquid air temperatures, of solid hydrates of some of the above salts have been reported.[3] These spectra consist of many bands, from about 20 cm^{-1} to about 150 cm^{-1} in width, extending throughout the visible region. Analysis indicates that these spectra may, in part, be interpreted in the same manner as those from the solutions. With $CoCl_2 \cdot 6H_2O$, the average wave number difference for twelve pairs of bands is 226 cm^{-1}. With $CoBr_2 \cdot 6H_2O$, the difference for ten pairs of bands is 220 cm^{-1}. For $NiCl_2 \cdot 6H_2O$, the difference for nine pairs of bands is 237 cm^{-1}. For $Co(OH_2)_6^{++}$, in passing from solution to the crystal, there is a decrease of 25 cm^{-1} in the separation of the vibrational bands. For $Ni(OH_2)_6^{++}$, there is a corresponding decrease of 27 cm^{-1}.

The interpretation presented here is consistent with the information obtained from the Raman effect of amino complex ions.[4] $Cu(NH_3)_4^{++}$, $Zn(NH_3)_6^{++}$, and $Cd(NH_3)_6^{++}$ give Raman displacements of the same order of magnitude as the separations of the vibrational levels of $Ni(NH_3)_6^{++}$ and the aquo complexes (see Table I). If one makes the approximation that the vibration of the complex ion may be represented by a simple harmonic oscillator, the force constant of the bond between the central metal ion and the coordinated group may be estimated from the vibration frequency. The values so obtained are listed in the table.

TABLE I.

Complex ion	Vibration frequency cm^{-1}	Force constant dynes/cm
$Cu(NH_3)_4^{++}$ (solution)	415 (Raman)	1.16×10^5
$Cd(NH_3)_6^{++}$ (solution)	340 (Raman)	0.85
$Zn(NH_3)_6^{++}$ (solution)	423 (Raman)	1.22
$Ni(NH_3)_6^{++}$ (solution)	390 (Absorption)	1.01
$Ni(OH_2)_6^{++}$ (solution)	264 (Absorption)	0.52
$Ni(OH_2)_6^{++}$ (crystal)	237 (Absorption)	0.42
$Co(OH_2)_6^{++}$ (solution)	248 (Absorption)	0.46
$Co(OH_2)_6^{++}$ (crystal)	223 (Absorption)	0.37
$Fe(OH_2)_6^{++}$ (solution)	324 (Absorption)	0.77

Some evidence for anharmonicity is obtained from a series of five bands for solid $CoCl_2 \cdot 6H_2O$.[3] The wave numbers of these bands may be represented with an accuracy of one wave number by:

$$\nu = 24504 + 222n - 1.6n^2 \quad (n = 0, \cdots, 4).$$

From the constants of this equation, the heat of dissociation of $Co(OH_2)_6^{++}$ in crystals of $CoCl_2 \cdot 6H_2O$ is estimated to be 22,000 cal. The heat of the reaction:

$$CoX_2 \cdot 6H_2O(s) \rightarrow CoX_2(s) + 6H_2O(l)$$

determined from thermochemical data (I.C.T.) is 21,300 cal. for $X = Cl$, 19,800 cal. for $X = Br$, and 16,700 cal. for $X = NO_3$. The decrease in the thermochemical value for the bromide as compared with the chloride parallels the decrease in the average separations of the vibrational levels, 226 cm^{-1} for the chloride as compared with 220 cm^{-1} for the bromide. The nitrate has not yet been studied spectroscopically.

[1] Th. Dreisch and W. Trommer, Zeits. f. physik. Chemie **B37**, 37 (1937).
[2] Th. Dreisch and O. Kallscheuer, Zeits. f. physik. Chemie **B45**, 19 (1939).
[3] Gieleszen, Ann. d. Physik [5] **22**, 537 (1935).
[4] I. Damaschun, Zeits. f. physik. Chemie **B16**, 81 (1932).